Srs2 binding to PCNA and its sumoylation contribute to RPA antagonism during the DNA damage response

Jiayi Fan[1], Nalini Dhingra[1#], Tammy Yang[2], Vicki Yang[2], Xiaolan Zhao[1]

[1]Molecular Biology Program, Memorial Sloan Kettering Cancer Center, New York, NY 10065

[2]City University of New York Hunter College, New York, NY 10065

Current address: Yale Center for Molecular Discovery, Yale University, West Haven, CT 06516

Corresponding author email: zhaox1@mskcc.org

Key words: DNA damage checkpoint, checkpoint dampening, Srs2, RPA, sumoylation, PCNA

Abstract

Activation of the DNA damage checkpoint upon genotoxin treatment induces a multitude of cellular changes, such as cell cycle arrest or delay, to cope with genome stress. After prolonged genotoxin treatment, the checkpoint can be downregulated to allow cell cycle and growth resumption. In yeast, downregulation of the DNA damage checkpoint requires the Srs2 DNA helicase, which removes the ssDNA binding complex RPA and the associated Mec1 checkpoint kinase from DNA, thus dampening Mec1-mediated checkpoint. However, it is unclear whether the 'anti-checkpoint' role of Srs2 is temporally and spatially regulated to both allow timely checkpoint termination and to prevent superfluous RPA removal. Here we address this question by examining regulatory elements of Srs2, such as its phosphorylation, sumoylation, and protein-interaction sites. Our genetic analyses and checkpoint level assessment suggest that the RPA countering role of Srs2 is promoted by Srs2 binding to PCNA, which recruits Srs2 to a subset of ssDNA regions. RPA antagonism is further fostered by Srs2 sumoylation, which we found depends on the Srs2-PCNA interaction. Srs2 sumoylation is additionally reliant on Mec1 and peaks after Mec1 activity reaches maximal levels. Based on these data, we propose a two-step model of checkpoint downregulation wherein Srs2 recruitment to PCNA proximal ssDNA-RPA filaments and subsequent sumoylation stimulated upon Mec1 hyperactivation facilitate checkpoint recovery. This model suggests that Srs2 removal of RPA is minimized at ssDNA regions with no proximal PCNA to permit RPA-mediated DNA protection at these sites.

Introduction

The DNA damage response promotes organismal survival of genotoxic stress by eliciting many cellular changes. A critical component of this response is a signaling process termed the DNA damage checkpoint (DDC) (Enoch *et al*, 1992; Hartwell and Weinert, 1989; Lanz *et al*, 2019). Upon encountering stress, apical DDC kinases are recruited to DNA lesion sites by the damage sensing proteins and are then activated by activator proteins (Usui *et al*, 2001; Zou and Elledge, 2003). A universal DDC sensor is the RPA complex that binds with high affinity and specificity to single-strand DNA (ssDNA), whose abundance rises under almost all types of genotoxic stress (Marechal and Zou, 2015). Using the budding yeast system as an example, RPA bound to the ssDNA filament can interact with Ddc2, the co-factor of the Mec1 checkpoint kinase, and recruit the Mec1-Ddc2 complex to DNA lesion sites (Elledge, 1996; Foiani *et al*, 2000). Subsequently, Mec1 is activated by activator proteins, such as the 9-1-1 complex loaded at the 5' DNA ends at ss-dsDNA junctions. Activated Mec1 can then phosphorylate multiple substrates, among which is a key downstream effector kinase Rad53, the phosphorylation of which turns on its own kinase activity and yields further phosphorylation events (Harrison and Haber, 2006). Collectively, the DDC kinases can modify hundreds of proteins, inducing multitude of pathway changes (Lanz *et al.*, 2019). For example, DDC can arrest or delay the cell cycle progression to allow more time for genome repair in promoting cellular survival (Sanchez *et al*, 1999; Wang *et al*, 2001).

While DDC activation is crucial for the cell to cope with genotoxic stress, its timely downregulation is equally vital (Waterman *et al*, 2020). Many changes induced by the DDC kinases need to be reversed to allow continued cell growth and recovery. For example, the DDC-mediated cell cycle arrest has to be lifted to allow proliferation and alternative DNA repair mechanisms permitted at other cell cycle phases (Pellicioli *et al*, 2001; Waterman *et al.*, 2020). Thus far, DDC downregulation has been mainly studied using the model organism yeast, with several strategies being identified (Waterman *et al.*, 2020). One of these is mediated by the DNA helicase Srs2 that targets the most upstream step of the DDC pathway through removing RPA and the associated Mec1-Ddc2 from chromatin (Dhingra *et al*, 2021). Importantly, the role of Srs2 in DDC dampening (anti-checkpoint) can be separated from its well-studied role in removing the recombinase Rad51 from ssDNA (anti-recombination) that modulates homologous recombination levels and outcomes (Dhingra *et al.*, 2021). The former role of Srs2 is critical for cell survival of genotoxins, such as camptothecin (CPT) that traps Top1 on DNA (Dhingra *et al.*, 2021). Considering that other organisms also possess DNA helicases capable of removing RPA from ssDNA (Hormeno *et al*, 2022; Jenkins *et al*, 2021; Shorrocks *et al*, 2021), it is plausible that an anti-checkpoint strategy involving RPA antagonism may be present beyond yeast.

Currently, little is known about how checkpoint dampening can be temporally controlled to minimize interference with the initial DDC activation that must occur in the early phase of the DNA damage response. In the case of the Srs2-mediated checkpoint regulation, it is also unclear how the process can minimize superfluous removal of RPA from ssDNA sites that unlikely induce the DDC due to lacking 5' DNA ends at ss-dsDNA junctions for 9-1-1 loading, such as at those formed at R-loops. The main functions of RPA at these sites can be ssDNA protection and repair, rather than DDC induction, thus these sites may benefit from shielding from Srs2-mediated RPA removal. In addressing these questions, we hypothesize that Srs2-based RPA antagonism should be selective in location and timing, and that the regulatory elements within the Srs2 protein may contribute to such selectivity.

To examine the above hypothesis and to define Srs2 features relevant to its RPA antagonism during DDC regulation, we inspected Srs2 protein sites involved in its post-

translational modifications and interactions with other proteins. Our genetic analyses of mutations affecting each of these sites suggest that while most of the examined features do not affect RPA antagonism, Srs2 binding to PCNA, which marks 3' DNA ends of ss-dsDNA junctions that flank ssDNA gaps or tails, and Srs2 sumoylation contribute to RPA regulation in the context of DDC. Srs2 binding to PCNA is known to recruit Srs2 to replication perturbation sites, while the roles of Srs2 sumoylation were less clear (Kolesar *et al*, 2012; Moldovan *et al*, 2007; Papouli *et al*, 2005; Pfander *et al*, 2005; Saponaro *et al*, 2010). Unexpectedly, we found that Srs2 binding to PCNA and Srs2 sumoylation are functionally related, since PCNA binding promotes Srs2 sumoylation. Moreover, Srs2 sumoylation level peaks late in the response to genomic stress after the DDC kinases are hyper-activated, and this modification depends on the Mec1 checkpoint kinase. Collectively, our data support a model wherein Srs2 can distinguish between two types of ssDNA regions using PCNA proximity as a guide for subsequent sumoylation, RPA removal, and countering hyper-activated checkpoint.

Results

Srs2 regulatory features and their disabling mutants

To understand which Srs2 attributes are relevant to RPA regulation during the DNA damage response, we examined mutant alleles that perturb known features of the Srs2 protein. Srs2 was reported to contain a helicase domain at its N-terminal region and three protein-protein interaction sites at its C-terminal region (Fig. 1A) (Niu and Klein, 2017). We have previously shown that the Srs2 ATPase-dead allele (*srs2-K41A*) fails to downregulate RPA levels on chromatin and Mec1-mediated DDC, indicating a requirement of ATPase-driven stripping of RPA from ssDNA (Dhingra *et al.*, 2021). The reported Srs2 protein-bindings sites include a Rad51 binding domain (Rad51-BD), a PCNA interaction motif (PIM), and a SUMO interaction motif (SIM) (Fig. 1A) (Colavito *et al*, 2009; Kolesar *et al*, 2016; Kolesar *et al.*, 2012). We employed CRISPR-based editing to generate the *srs2-ΔPIM* (Δ1159-1163 amino acids) and the *srs2-SIM*^{mut} ($_{1170}$IIVID$_{1174}$ to $_{1170}$AAAAD$_{1174}$) alleles used in previous studies and examined an established *srs2-ΔRad51BD* allele (Δ875-902 amino acids) (Colavito *et al.*, 2009; Kolesar *et al.*, 2016; Kolesar *et al.*, 2012). We note that despite Srs2 removal of RPA from ssDNA, an interaction between the two proteins has yet to be reported.

We also queried post-translational modifications reported for Srs2 by mutating the corresponding modification sites (Fig. 1A). First, seven Cdk1 phosphorylation consensus sites of Srs2 were mutated to produce the *srs2-7AV* (T604V, S698A, S879A, S893A, S938A, S950A, and S965A) allele (Chiolo *et al*, 2005), which was previously shown to affect homologous recombination. Second, three sumoylation sites of Srs2 were mutated to generate *srs2-3KR* (K1081R, K1089R, and K1142R) (Saponaro *et al.*, 2010). Finally, we mutated two serine residues (S890 and S933) to alanine to generate *srs2-2SA*, since phosphorylation at these sites was identified in proteomic studies as dependent on both the Mec1 kinase and genotoxic treatments (Faca *et al*, 2020). Because the Srs2 C-terminal end contributes to the protein's functions (Antony *et al*, 2009; Colavito *et al.*, 2009), the six mutant alleles described above were not tagged with epitopes at its C-terminus. Using an anti-Srs2 specific antibody, we showed that all six alleles supported wild-type levels of Srs2 protein based on immunoblotting (Fig. 1B).

Mutating PCNA binding and sumoylation sites of Srs2 rescues *rfa1-zm2* CPT sensitivity

Srs2 loss leads to persistent DDC and perturbed recombination, both of which contribute to *srs2*Δ sensitivity to genotoxins, including CPT and methyl methanesulfonate (MMS) (Fig. 2A) (Niu and Klein, 2017). Significantly, our recent study has shown that RPA mutants that reduce its ssDNA binding affinity rescue the persistent DDC levels in *srs2*Δ cells but not their recombination defects (Dhingra *et al.*, 2021). *rfa1-zm2* (N492D, K493R, K494R) is one of the RPA alleles examined that contains mutations at three DNA contacting residues in the Rfa1 subunit of RPA (Fan and Pavletich, 2012). Purified RPA complex containing these mutations exhibited a two-fold increase in dissociation constant using ssDNA as substrate, compared to the wild-type RPA complex (Dhingra *et al.*, 2021). In cells, *rfa1-zm2* supports normal Rfa1 protein level, cell growth, DNA replication (Dhingra *et al.*, 2021). It also did not affect gene conversion, direct repeat repair or rDNA recombination, nor the hyper-recombination phenotype of *srs2*Δ (Dhingra *et al.*, 2021). However, *rfa1-zm2* and *srs2*Δ are mutually suppressive for both their genotoxic sensitivities and their DDC abnormalities (Fig. 2B, S1A) (Dhingra *et al.*, 2021). These data suggest that the *srs2* and *rfa1-zm2* genetic relationship can be used as a readout for the antagonism between Srs2 and RPA in DDC and that this functional relationship can be separable for Srs2's anti-recombination role stemming from Rad51 regulation. Based on this rationale, we employed the genetic suppression as an initial readout in querying whether any of the six *srs2* mutant alleles described above are related to RPA regulation. Given that Srs2's role in checkpoint dampening was best examined in CPT (Dhingra *et al.*, 2021), which induces the DNA damage checkpoint to delay G2/M progression, but does not induce the DNA replication checkpoint, experiments were mostly carried out in this condition.

We found that on their own, *srs2-SIM*^{mut}, -Δ*PIM*, and *-7AV* showed different levels of sensitivity toward CPT at a concentration ranging from 2 to 8 µg/ml, while *srs2-*Δ*Rad51BD* and *-3KR* exhibited close to wild-type level of CPT resistance, which are consistent with previous reports (Colavito *et al.*, 2009; Saponaro *et al.*, 2010) (Fig. S1A). In addition, *srs2-2SA,* which has not been examined previously, did not show CPT sensitivity (Fig. S1A). Since *rfa1-zm2* cells exhibited stronger CPT sensitivity than the tested *srs2* alleles (Fig. S1A), we asked if the latter could suppress *rfa1-zm2* CPT sensitivity. We found that both *srs2-*Δ*PIM* and *-3KR* improved the CPT resistance of *rfa1-zm2* cells on media containing 2 µg/ml CPT (Fig. 2C). Rescue was also seen at higher CPT concentrations, with *srs2-*Δ*PIM* exhibiting a stronger effect than *srs2-3KR* (Fig. S1B). In contrast to *srs2-*Δ*PIM* and *srs2-3KR*, *srs2-*Δ*Rad51BD* and *-2SA* showed no effect on *rfa1-zm2* growth on media containing CPT, whereas *srs2*-7AV *and -SIM*^{mut} worsened it (Fig. 2D). The differential effects seen for the *srs2* alleles are consistent with the notion that Srs2 has multiple roles in cellular survival of genotoxic stress (Bronstein *et al*, 2018; Niu and Klein, 2017). The unique suppression seen for mutants affecting Srs2 binding to PCNA and its sumoylation suggests that these features are relevant to RPA regulation during the DNA damage response.

Additional suppressive effects conferred by *srs2-*Δ*PIM* and *-3KR* toward *rfa1* mutants

We next tested whether the observed *srs2-*Δ*PIM* and *-3KR* suppression was specific towards *rfa1-zm2* or applicable to other *rfa1* mutants that are also defective in ssDNA binding. While *rfa1-zm2* affects the ssDNA binding domain C (DBD-C) of Rfa1, a widely used *rfa1* allele, *rfa1-t33,* impairs the DBD-B domain (Fig. 2E) (Umezu *et al*, 1998). Unlike *rfa1-zm2, rfa1-t33* additionally decreases Rfa1 protein level and interferes with DNA replication and repair (Deng *et al*, 2014; Umezu *et al.*, 1998). Despite having these additional defects, CPT survival of *rfa1-t33* cells was also improved by *srs2-*Δ*PIM* or *srs2-3KR* (Fig. 2E). As seen in the case of *rfa1-zm2*, *srs2-*Δ*PIM* conferred better rescue than *srs2-3KR* toward *rfa1-t33* (Fig. 2E). When comparing the two *rfa1* alleles, *srs2* rescue was stronger toward *rfa1-zm2*, likely because *rfa1-t33* has

other defects besides reduced ssDNA binding (Fig. 2C, 2E). In either case, *srs2* mutants only conferred partial suppression, consistent with the notion that Srs2 has roles beyond RPA regulation (Bronstein *et al.*, 2018; Niu and Klein, 2017). Nevertheless, the observed rescue of both *rfa1-zm2* and *rfa1-t33* provided strong genetic evidence that Srs2 binding to PCNA and sumoylation are involved the regulation of RPA during the DNA damage response.

Srs2 regulation of RPA during DDC is not only observed under CPT treatment, but is also seen in treatment with MMS (Dhingra *et al.*, 2021), which induces both DDS and the DNA replication checkpoint and thus delaying both S phase progression and G2/M phase exit (Paciotti *et al*, 2000; Tercero *et al*, 2003). Consistent with observation made in CPT conditions, *srs2-ΔPIM* moderately improved the MMS sensitivity of *rfa1-zm2* and *rfa1-t33,* while *srs2-3KR* had a small effect on the MMS sensitivity of *rfa1-zm2* (Fig. S1B, S1C). The degrees of suppression seen in MMS treatment were less than those observed in CPT conditions, and we address likely reasons for this difference in Discussion. Collectively, the multiple genetic results are consistent among themselves and provide evidence that the roles of Srs2 binding to PCNA and sumoylation in RPA antagonism can be applicable to more than one genomic stress situation.

srs2-ΔPIM and *-3KR* rescue checkpoint abnormality of *rfa1-zm2* cells

We next investigated whether *srs2-ΔPIM* and *-3KR* suppression of the DNA damage sensitivity of *rfa1-zm2* cells pertained to DDC regulation. We employed two readouts for DDC that are widely used. First, we used the F9 antibody, which specifically recognizes phosphorylated Rad53, to measure the levels of activated Rad53 (Fiorani *et al*, 2008). Second, we measure cellular ability to timely exit the G2/M phase after CPT treatment using FACS analyses. We note that CPT-induced DDC leads to G2/M delay rather than an arrest as shown in previous studies (Dhingra *et al.*, 2021; Menin *et al*, 2018; Redon *et al*, 2003). We have recently reported that *srs2Δ* cells exhibit increased levels of phosphorylated Rad53 and diminished ability to timely exit G2/M phase in CPT, and that both are suppressed by *rfa1-zm2* (Dhingra *et al.*, 2021; Menin *et al.*, 2018; Redon *et al.*, 2003). Interestingly, *rfa1-zm2* leads to similar defects and these are rescued by *srs2Δ* (Dhingra *et al.*, 2021) (Fig. 3A). The mutual suppression seen in these assays is consistent with that seen for CPT sensitivity (Dhingra *et al.*, 2021). We note that several other RPA ssDNA binding mutants, such as *rfa1-t33*, also exhibit phenotypes indicative of increased DDC levels (Pellicioli *et al.*, 2001; Seeber *et al*, 2016; Smith and Rothstein, 1995; Zou and Elledge, 2003). This is likely because compromised ssDNA protection can lead to increased levels of DNA lesions thus enhancing the activation of Mec1 and/or its homolog Tel1.

We reasoned that if *srs2-ΔPIM* and *srs2-3KR* compromise Srs2's ability to remove RPA from DNA in cells, they should alleviate *rfa1-zm2* cells' defects in ssDNA protection and the associated DDC abnormalities (Fig. 3A). Indeed, while *rfa1-zm2* exhibited about 5-fold increase in Rad53 phosphorylation levels in CPT compared with wild-type cells as seen before (Dhingra *et al.*, 2021), *srs2-ΔPIM* and *-3KR* reduced this level by about 50% and 80%, respectively (Fig. 3B). Similar to earlier data, we observed that wild-type cells arrested in G_2/M after 1 hour of CPT treatment and about 25% of these cells entered G_1 after another hour (Fig. 3C) (Dhingra *et al.*, 2021). The ability to timely exit from G_2/M phase was reduced in *rfa1-zm2* cells so that only 13% cells moved to G1 phase after 2 h treatment with CPT, as seen before (Fig. 3C) (Dhingra *et al.*, 2021). Significantly, *srs2-ΔPIM* and *-3KR* increased the percentage of *rfa1-zm2* cells transitioning into the G1 phase (Fig. 3C). The suppressive effects seen in both assays were stronger for *srs2-ΔPIM* than *srs2-3KR* as seen in genotoxicity assays (Fig. S1B; 3B, 3C).

Collectively, the genetic and DDC assay data are consistent with each other and suggest that Srs2 binding to PCNA and its sumoylation contribute to RPA antagonism in DDC regulation.

srs2-ΔPIM is additive with a *slx4* mutant defective in DDC recovery

We found that *srs2-ΔPIM* and *srs2-3KR* mutants on their own behaved normally in the two DDC assays described above, which differs from *srs2Δ* cells that exhibit increased levels of Rad53 phosphorylation and reduced G1 entry (Fig. 3B, 3C) (Dhingra *et al.*, 2021). One plausible interpretation of this difference is that unlike *srs2Δ*, these partially defective *srs2* mutants only mildly impair Srs2-mediated RPA regulation during DDC downregulation, such that their defects can be compensated for by other DDC dampening systems. To test this idea, we examined the consequences of removing the Slx4-mediated anti-checkpoint function in *srs2-ΔPIM* cells. Slx4 is known to bind the scaffold protein Rtt107, and their complex can compete with the DDC protein Rad9 for binding to damaged chromatin, consequently disfavoring Rad9's role in promoting Rad53 phosphorylation (Ohouo *et al*, 2010; Ohouo *et al*, 2013). Slx4 uses an Rtt107 interaction motif (RIM) to bind Rtt107 and a previously established RIM mutant, $slx4^{RIM}$ (T423A, T424A, and S567A), abolishes Rtt107 binding without affecting other Slx4 protein attributes (Wan *et al*, 2019). $slx4^{RIM}$ was tagged with a TAP tag at its C-terminal end and examined together with a control wherein the wild-type Slx4 was tagged in the same manner. Compared with the control, $slx4^{RIM}$ exhibited mild sensitivity toward CPT (Fig. 4A). Significantly, when *srs2-ΔPIM* was combined with $slx4^{RIM}$, the double mutant exhibited stronger CPT sensitivity compared with corresponding single mutants (Fig. 4A).

We further examined DDC levels when cells were exposed to CPT using both Rad53 phosphorylation and ability to timely exit G2/M as readouts. Compared with *Slx4-TAP* cells, $slx4^{RIM}$*-TAP* cells exhibited 2-fold increase in Rad53 phosphorylation level, consistent with a role of Slx4 in downregulating DDC (Fig. 4B). In *Slx4-TAP* background, *srs2-ΔPIM* led to 3-fold increase in Rad53 phosphorylation level (Fig. 4B). As cells containing untagged Slx4 and *srs2-ΔPIM* did not show Rad53 phosphorylation changes (Fig. 3B), tagging Slx4 likely sensitizes *srs2-ΔPIM.* Significantly, the double mutant of *srs2-ΔPIM* and $slx4^{RIM}$*-TAP* exhibited further increase in Rad53 phosphorylation (~5.5 fold) compared with *srs2-ΔPIM* and $slx4^{RIM}$*-TAP* single mutant (Fig. 4B). Congruous with this finding, the *srs2-ΔPIM* $slx4^{RIM}$*-TAP* double mutant also reduced the percentage of cells entering G_1 compared with their single mutants after 2-hour treatment with CPT (Fig. 4C). Together, these three lines of evidence support the notion that defects in the Srs2-mediated DDC downregulation can be compensated for by Slx4-mediated mechanisms.

Srs2 binding to PCNA facilitates Srs2 sumoylation

We next addressed whether the two Srs2 features involved in RPA antagonism are functionally related. To this end, we tested if Srs2 binding to PCNA affected Srs2 sumoylation in cells. We confirmed that endogenous sumoylation of Srs2 could be detected in cell extracts after enriching SUMOylated proteins using 8His-tagged SUMO (8His-Smt3) (Fig. 5A). Briefly, proteins were extracted from cells under denaturing conditions to disrupt protein-protein association and prevent desumoylation, and sumoylated proteins were enriched on Ni-NTA (nickel-nitrilotriacetic acid) resin (Ulrich and Davies, 2009). Consistent with previous findings, sumoylated forms of Srs2 in the Ni-NTA eluate were detected on immunoblots using an anti-Srs2 antibody only when cells contained 8His-Smt3, where unmodified Srs2 was seen in the presence or absence of 8His-Smt3 due to nonspecific binding to the resin (Fig. S2A) (Saponaro

et al., 2010). These bands were only seen in wild-type cells but not *srs2*Δ cells (Fig. S2A). We found that Srs2 sumoylation level was reduced in *srs2-3KR* strains in CPT conditions, as expected from mutating the three major sumoylation sites (Fig. 5A) (Saponaro *et al.*, 2010). Interestingly, *srs2-ΔPIM* cells exhibited a similar reduction in Srs2 sumoylation as seen in *srs2-3KR* cells (Fig. 5A). This result suggests that Srs2 sumoylation largely depends on Srs2 binding to PCNA, supporting the notion that the two events occur sequentially.

Srs2 sumoylation peaks after maximal Mec1 activation and depends on Mec1

While RPA can engage with ssDNA generated in different processes, such as transcription, DNA repair, and DNA replication, only a subset of ssDNA regions is adjacent to 3'-junctions loaded with PCNA. This is because PCNA loading requires an ssDNA and dsDNA junction site with a 3' DNA end and occurs mainly during S phase (Moldovan *et al.*, 2007). We thus reasoned that Srs2 binding to PCNA may prevent Srs2 from removing RPA bound to ssDNA that forms transiently or is not flanked by PCNA, such as within R-loop regions and negatively supercoiling DNA regions, both of which are generated abundantly in CPT conditions due to topological stress (Pommier *et al*, 2022). This could provide a means for spatial control of Srs2's anti-RPA role. We explored whether this role could also be regulated temporally. As the genetic data described above suggest that Srs2 sumoylation acts downstream of Srs2 binding to PCNA in antagonizing RPA, we examined the timing of Srs2 sumoylation after CPT treatment.

We released G1 synchronized cells into media containing CPT and examined Srs2 sumoylation at several time points (Fig. 5B). A similar experimental scheme was used to monitor the level of Mec1 activation using Rad9 phosphorylation as a readout (Fig. 5C). Quantification of Srs2 sumoylated forms relative to its unmodified forms showed that its sumoylation level peaked between 1.5 and 2 h after cells were released into CPT (Fig. 5D). Quantification of phosphorylated forms of Rad9 relative to its unmodified form showed that checkpoint activation peaked 1 hour after cell release (Fig. 5D). That checkpoint level peaked before Srs2 sumoylation level peaked suggests a possible dependence of the latter on the checkpoint. In testing this idea, we found that *mec1*Δ cells, which contain *sml1*Δ to support viability (Zhao *et al*, 1998), abolished Srs2 sumoylation (Fig. 5E). Neither *sml1*Δ alone nor removal of Rad53 affected Srs2 sumoylation (Fig. 5E), suggesting that Mec1's effect on this modification does not require the downstream Rad53 effector kinase. As Mec1 is not generally required for protein sumoylation during the DNA damage response (Cremona *et al*, 2012), its involvement in Srs2 sumoylation presents a rather unique effect.

Examination of Mec1-S1964 phosphorylation in Srs2-mediated DDC regulation

The combined results that Srs2 sumoylation levels peak after Rad9 phosphorylation reaches maximal level and that Srs2 sumoylation depends on Mec1 raised the possibility that Mec1 hyper-activation during the late part of the DNA damage response may favor Srs2's role in DDC dampening. Recently, Mec1 protein bound to Ddc2 was shown to be auto-phosphorylated at Ser1964 in a late part of the DNA damage response after a single DNA break is induced by the HO endonuclease (Memisoglu *et al*, 2019). Further, the phosphorylation-defective mutant *mec1-S1964A* impaired checkpoint downregulation in this condition, leading to the model that Mec1-S1964 phosphorylation contributes to DDC dampening at least after HO-induced break (Memisoglu *et al.*, 2019). We thus tested whether Mec1-S1964 phosphorylation is also involved in Srs2-mediated DDC regulation under CPT conditions.

First, we asked whether Mec1-S1964 phosphorylation occurs under CPT conditions using a time course scheme similar to the one used in testing Srs2 sumoylation as described above. Ddc2-bound Mec1 was recovered after immunoprecipitating Ddc2 at each timepoint and the proteins were examined by immunoblotting. To detect Mec1-S1964 phosphorylation, we used an antibody raised against the peptide containing this modification provided kindly by the Haber lab (Memisoglu *et al.*, 2019). The antibody detected the Mec1 S1964 phosphorylation band in immunoprecipitated fractions only when Ddc2 was tagged with the Myc tag but not when Ddc2 was untagged (Fig. S2B). Further, the Mec1 S1964 phosphorylation band was largely abolished in the *mec1-S1964A* cells. (Fig. S2B; 6A). Given that the antibody also detects a closely spaced background band (Fig. S2B; 6A), we calculated the relative level of Mec1 S1964 phosphorylation in each sample by normalizing to this band. Quantification results showed that Mec1 S1964 phosphorylation level peaked around the same time as seen for Rad9 phosphorylation, which was 1 hour after CPT treatment (Fig. 6A).

After confirming that Mec1 S1964 phosphorylation also took place under CPT conditions, we tested whether the *mec1-S1964A* or the phosphorylation-mimetic mutant, *mec1-S1964E*, influenced *rfa1-zm2* or *srs2* growth on media containing CPT. If Mec1 S1964 phosphorylation aids Srs2-mediated RPA antagonism in CPT, we would expect *mec1-S1964A* to behave similarly to *srs2* mutants in rescuing *rfa1-zm2* CPT sensitivity, while *mec1-S1964E* should have the opposite effects. We found that *mec1-S1964A,* which showed normal CPT resistance on its own, did not affect the growth of *rfa1-zm2* cells on CPT-containing media (Fig. 6B). *mec1-S1964A* also did not influence the growth of *srs2-ΔPIM* and *srs2-3KR* cells regardless of *rfa1-zm2* (Fig. 6B; S3A).

Though *mec1-S1964E* on its own did not cause CPT sensitivity*,* it led to slight but reproducible slow growth in cells containing *srs2-3KR* and *srs2-ΔPIM* with or without *rfa1-zm2* (Fig. S3B). We found that neither *mec1-S1964A* nor *mec1-S1964E* affected Srs2 sumoylation levels (Fig. S3C). Thus, Mec1, but not its S1964 phosphorylation, is required for Srs2 sumoylation. These data provide evidence that even though an HO-induced DNA break and CPT treatment both induce Mec1 S1964 phosphorylation, this modification appears to not affect Srs2-mediated DDC dampening in the latter situation.

Genetic data suggest that known RPA phosphorylation sites do not affect DDC recovery

While we mainly focused on the identification of Srs2 features that contribute to RPA antagonism during DDC regulation, we also considered the possibility that certain regulatory RPA features may contribute to this control as well. In particular, RPA is known to be phosphorylated by Mec1 (Chen *et al*, 2010; Faca *et al.*, 2020; Lanz *et al*, 2021). We thus tested whether Mec1-mediated phosphorylation may render RPA more susceptible to be removed from ssDNA by Srs2. To this end, we mutated previously identified Mec1 phosphorylation sites on the Rfa1 and Rfa2 subunits. These include Rfa1 Ser178 and three sites on Rfa2 (S122, S187, S189) (Albuquerque *et al*, 2015; Chen *et al.*, 2010). We generated corresponding non-phosphorylatable mutants, *rfa1-S178A* and *rfa2-3SA (*S122A, S187A, and S189A), and phosphomimetic mutants, *rfa1-S178D* and *rfa2-3SD*.

Using genetic suppression as a readout for possible involvement of RPA mutants in Srs2-based DDC regulation, we examined the interactions between the mutants affecting RPA phosphorylation sites as described above and *srs2*Δ. If RPA phosphorylation promote its removal by Srs2, the *SD* mutants may show suppressive interactions with *srs2*Δ, while *SA* mutants would behave like *srs2* mutants. We found that neither *rfa1-S178D* nor *S178A*, both of

which showed normal CPT resistance on their own, affected *srs2*Δ cell growth on CPT-containing media (Fig. 6C). In contrast, *rfa2-3SD* or *rfa2-3SA,* which also behaved like wild-type regarding CPT sensitivity, sensitized *srs2*Δ growth on CPT-containing media (Fig. 6D). This negative genetic interaction contrasts with the positive interaction seen between *srs2*Δ and *rfa1-zm2* or *rfa1-t33* (Fig. S1A) (Dhingra *et al.*, 2021). The differential Srs2 genetic interactions among distinct RPA alleles likely reflect the multifunctional natures of Srs2 and RPA. Collectively, these analyses suggest that the known phosphorylation sites on RPA are unlikely to be involved in Srs2-based DDC regulation.

Discussion

Timely termination of DDC is crucial for cell survival, yet the underlying mechanisms are not well understood. Using the budding yeast model system, we investigated how the Srs2-mediated DDC dampening through antagonizing RPA can be regulated. Our previous work reports a requirement of Srs2's ATPase activity in this role; here we examined additional Srs2 features involved in either binding to other proteins or post-translational modifications. Our results suggest that among the examined features, Srs2 binding to PCNA and its sumoylation are involved in RPA antagonism during DDC downregulation. We showed that mutants impairing these features, namely *srs2*Δ*-PIM* and *srs2-3KR*, suppressed both DDC abnormalities and CPT sensitivity of *rfa1-zm2* cells. Interestingly, these features are functionally linked, since optimal Srs2 sumoylation requires its binding to PCNA. Further, the Srs2 sumoylation level peaks after Mec1 activity reaches its maximum and that Mec1 is required for this modification. We posit a model that can interpret previous and current data. In this model, Srs2 removal of RPA is favored at a subset of ssDNA regions that have proximal PCNA (Fig. 7, top). PCNA recruits Srs2 toward the adjacent RPA-ssDNA filament, and promotes Srs2 sumoylation together with hyperactive Mec1, and both effects foster downregulation of the Mec1 checkpoint (Fig. 7, bottom).

RPA-ssDNA filaments can be separated into two groups based on PCNA loading status. The first group contains 3' DNA end at the ss-dsDNA junction to permit PCNA loading (Fig. 7, top, green). These regions can include ssDNA gaps produced from perturbed replication (Sogo *et al*, 2002)or from excision and repair of trapped Top1 (Sun *et al*, 2020). Due to PCNA proximity, this group of ssDNA regions can favor Srs2 recruitment and RPA removal. Since they often also contain 5' DNA ends required for loading the 9-1-1 complex (Majka *et al*, 2006), these sites can be ideal for Srs2's action in checkpoint dampening. The second group of ssDNA regions are devoid of 3' DNA end thus PCNA loading. These regions can be within R-loops or negatively supercoiled regions, which are induced by CPT treatment due to increased topological stress associated with the depletion of the functional pool of Top1 (Pommier *et al.*, 2022). These regions are unlikely to contain 5' DNA ends at ss-dsDNA junctions; thus RPA there mainly supports DNA protection and repair and not DDC. We reason that these ssDNA sites can be shielded from Srs2 removal of RPA to allow better repair and protection. The notion that ssDNA regions close to PCNA are preferred for Srs2 anti-checkpoint action provides a rationale for how Srs2 could remove RPA at some sites and minimize unnecessary RPA loss from other sites. Quantitative assessment of RPA residence on DNA and genome-wide mapping of Srs2 action sites in the future can further test the proposed models and provide more clarity. Regardless, results presented in this work support the conclusion that Srs2 can distinguish between two types of ssDNA regions using PCNA proximity as a guide for RPA removal.

Genetic analysis showed that *srs2Δ-PIM* also suppressed *rfa1-zm2* sensitivity toward MMS, though to a less degree as seen in CPT conditions. While more than one factor could contribute to this difference, we note that CPT only activates the DNA damage checkpoint, while MMS additionally induces DNA replication checkpoint (Menin *et al.*, 2018; Redon *et al.*, 2003; Tercero *et al.*, 2003). It is thus possible that the Srs2-RPA antagonism is more important for the DNA damage checkpoint compared with the DNA replication checkpoint. Further investigation of this possibility among others will shed light on differential suppressive effects seen here.

An involvement of PCNA binding in Srs2-based RPA regulation could compensate for a lack of Srs2 interaction with RPA. This scenario differs from Srs2-based Rad51 stripping that requires their interaction (Antony *et al.*, 2009; Colavito *et al.*, 2009; Krejci *et al*, 2003). It is thus likely that though both the anti-recombinase and anti-checkpoint roles of Srs2 benefit from selectivity, they are achieved via different means. Our previous work has provided several lines of evidence to support that Rad51 removal by Srs2 is separable from the Srs2-RPA antagonism (Dhingra *et al.*, 2021). Consistent with this conclusion, deleting the Rad51 binding domain in Srs2 had no effect on *rfa1-zm2* phenotype in CPT (Fig. 2D). This is in sharp contrast to mutating the PCNA binding and the sumoylation sites of Srs2, which suppressed *rfa1-zm2* defects (Fig. 2C). This data provides additional evidence that Srs2 regulation of Rad51 is separable from the Srs2-RPA antagonism. For this reason, the Srs2-based Rad51 function was not further examined in this study. However, future studies to address how Srs2 regulates RPA and Rad51 in different manners and whether there is a crosstalk between them in specific contexts will help to generate a more comprehensive understanding of the Srs2's anti-checkpoint vs. anti-recombination functions.

Previous studies have suggested that both PIM and SIM aid Srs2 recruitment to sumoylated form of PCNA (Papouli *et al.*, 2005; Pfander *et al.*, 2005). Our data reveal that at least in CPT conditions, Srs2-PIM, but not Srs2-SIM, is involved in RPA regulation. This observation is congruent with phenotypic differences between Srs2's PIM and SIM seen in other studies and here, such as much stronger genotoxic sensitivity of the latter (Fig. S1A) (Fan *et al*, 2023; Kolesar *et al.*, 2016; Kolesar *et al.*, 2012). Considering that only a small percentage of PCNA is sumoylated and mainly during S phase (Papouli *et al.*, 2005; Pfander *et al.*, 2005), it is probably advantageous for Srs2 not being restricted to sumoylated PCNA in order to achieve efficient RPA regulation.

How could Srs2 binding to PCNA helps Srs2 sumoylation? While a full answer awaits future studies, we speculate that this interaction may render Srs2 more permissive for sumoylation and/or position Srs2 in proximity with its sumoylation E3 ligase Siz2 that binds RPA (Chung and Zhao, 2015; Kolesar *et al.*, 2012). Considering that Mec1, Ddc2, and RPA contain SUMO interaction motifs (Psakhye and Jentsch, 2012), it is possible that Srs2 sumoylation could help enrich the helicase at ssDNA-RPA sites via interacting with these motifs, though other effects are also possible. Compared with *srs2-3KR*, *srs2-ΔPIM* showed better suppression of *rfa1-zm2* defects. This indicates that during RPA regulation, PCNA plays additional roles besides promoting Srs2 sumoylation.

We found that Srs2 sumoylation in cells also requires Mec1, which does not promote sumoylation in general (Cremona *et al.*, 2012). On the contrary, Mec1 loss causes increased sumoylation levels (Cremona *et al.*, 2012). It is currently unclear how Mec1 can specifically promote Srs2 sumoylation, but this may involve Mec1-mediated phosphorylation of SUMO substrates and/or enzymes. A requirement of Mec1 for Srs2 sumoylation and the dynamic nature of sumoylation suggest that Srs2 sumoylation may be a potential timing regulator. It is possible that hyperactivation of Mec1 favors Srs2 sumoylation that may aid its own

downregulation. While fully testing this idea requires time-course phosphor-proteomic studies under genotoxin treatment, we examined a Mec1 auto-phosphorylation site implicated in its downregulation after induction of a single DNA break (Memisoglu *et al.*, 2019). We did not find evidence that it is involved in Mec1 dampening in CPT condition, raising the possibility that distinct mechanisms may be used in different genomic stress conditions. We also found that two phosphorylation sites on Srs2 that showed Mec1 dependency in proteomic studies had no effect in the CPT situation (Albuquerque *et al.*, 2015; Faca *et al.*, 2020); however we note that these sites do not fit with the typical S/TQ Mec1 consensus sites, thus may not be the bona fide Mec1 sites. Other phosphorylation sites examined here include five Mec1 sites on Rfa1 and Rfa2 (Albuquerque *et al.*, 2015; Chen *et al.*, 2010). Genetic analyses did not support their roles in the Srs2 and RPA antagonism. Thus, future studies to comprehensively map DDC kinase phosphorylation sites on Srs2 and RPA, as well as their regulators, such as the RPA chaperone Rtt105 (Li *et al*, 2018), will be needed to test how the kinases can communicate with Srs2-based RPA regulation during the DNA damage response.

While we provide multiple lines of evidence in support of the involvement of Srs2 binding to PCNA and its sumoylation in RPA regulation during DDC downregulation, *srs2-ΔPIM* or *-3KR* alone behaved normally in checkpoint assays. A lack of defect here can be due to buffering effects, both from not-yet characterized Srs2 features and from other checkpoint dampening pathways. In addressing the former possibility, we tested the separation pin of Srs2 (Y775), which was shown to enables its *in vitro* helicase activity during the revision of our work (Meir *et al*, 2023). We found that the *srs2-Y775A* mutation that severely compromised the Srs2 helicase activity rescued *rfa2-zm2* sensitivity to CPT (Fig. S4). This result suggests that Y775 may directly contribute to *in vivo* RPA removal; future examination of this feature, alone and in conjunction with PCNA binding and sumoylation, can extend our understanding of Srs2-mediated DDC regulation. We also provided evidence for the latter possibility, since *srs2-ΔPIM* or *-3KR* showed additive phenotype when combined with a *slx4* mutant defective in DDC dampening function. The presence of multiple checkpoint dampening factors that target different checkpoint modules highlights the importance of the process. Recent demonstration of other DNA helicases, such as the human HELB, HELQ, and BLM proteins, in stripping of RPA from ssDNA in vitro suggests that Srs2-like checkpoint downregulation may present in human cells as well (Hormeno *et al.*, 2022; Jenkins *et al.*, 2021; Shorrocks *et al.*, 2021). Since RPA-ssDNA binding not only plays a key role in checkpoint, but also in many other processes, the Srs2 features uncovered here may help to better understand how RPA dynamics is controlled by helicases and other factors during additional processes beyond DDC.

Methods

Yeast strains and genetic techniques. Standard procedures were used for cell growth and media preparation. The strains used in this work are listed in Table S1and are isogenic to W1588-4C, a *RAD5* derivative of W303 (Zhao and Blobel, 2005). Mutant alleles of *srs2*, *rfa1*, *rfa2* and *mec1* used in this work were generated by CRISPR-Cas9-based gene replacement, except for *srs2-3KR* that was introduced using a PCR-based method (DiCarlo *et al*, 2013). All mutations were verified by sequencing. Standard procedures were used for tetrad analyses and genotoxin testing. For each assay, at least two biological duplicates were used per each genotype. Cells were grown at 30 ºC unless otherwise stated.

Cell synchronization and cell cycle analyses. Cells from log-phase cultures were treated with 5 μg/mL α factor (GenScript RP01002) for 1 h, followed by an additional 2.5 μg/mL α factor for 30 min. When at least 95% cells were arrested in G1 phase based on the percentage of

unbudded cells, they were released into yeast extract–peptone–dextrose (YPD) media containing 100 µg/mL Protease (Millipore 53702) and 16 µg/mL CPT (Sigma C9911) for 2 h. Cell cycle progression was monitored by standard flow cytometry analyses as described previously (Zhao and Rothstein, 2002). To derive percentage of G1 cells in Figure 3B, the G1 region of the "G1 sample" was used to demarcate the G1 region of the "CPT 2h" sample of the same strain in the same experiment.

Protein extraction using trichloroacetic acid (TCA). To examine the protein levels of Srs2, the phosphorylation form of Rad53, and Rad9, cell extracts were prepared as reported (Regan-Mochrie *et al*, 2022) . Briefly, 2×10^8 cells were collected at indicated time points. Cell pellets were resuspended in 20% TCA and lysed by glass bead beating. The lysate was then centrifuged to remove supernatant. Precipitated proteins were suspended in Laemmli buffer (65 mM Tris-HCl at pH 6.8, 2% SDS, 5% 2-mercaptoethanol, 10% glycerol, 0.025% bromophenol blue) with 2 M Tris added to neutralize the solution. Prior to loading, samples were boiled for 5 min and spun down at 14,000 rpm for 10 min to remove insoluble materials. Samples were separated on 4-20% Tris-glycine gels (Bio-Rad 456-1096) to examine Srs2 level and phosphorated Rad53 form or 7% Tris-acetate gels (Thermo Fisher EA03555) to detect Rad9 phosphorylation.

Detection of Srs2 sumoylation. Sumoylated proteins were pulled down from cells containing 8His-tagged SUMO expressed from its endogenous locus using the standard Ni-NTA pull-down method as previously described (Ulrich and Davies, 2009). Briefly, protein extracts prepared in 55% TCA were incubated in buffer A (6 M guanidine HCl, 100 mM sodium phosphate at pH 8.0, 10 mM Tris-HCl at pH 8.0) with rotation for 1 h at room temperature. The cleared supernatant was obtained after centrifuging for 20 min and was then incubated overnight at room temperature with Ni-NTA resin (Qiagen 30210) in the presence of 0.05% Tween-20 and 4.4 mM imidazole with rotation. Beads were washed twice with buffer A supplemented with 0.05% Tween 20 and then four times with buffer C (8 M urea, 100 nM sodium phosphate at pH 6.3, 10 mM Tris-HCl at pH 6.3) supplemented with 0.05% Tween 20. Proteins were eluted from the beads using HU buffer (8 M urea, 200 mM Tris-HCl at pH 6.8, 1 mM EDTA, 5% SDS, 0.1% bromophenol blue, 1.5% DTT, 200 mM imidazole). Samples were loaded onto NuPAGE™ 3–8% Tris-acetate gels (Thermo Fisher EA03752) for immunoblotting to detect both sumoylated and unmodified Srs2. Equal loading was verified using Ponceau S staining.

Detection of Mec1 S1964 phosphorylation during CPT treatment. G1-arrested cells were filtered and resuspended in prewarmed YPD media containing 16 µg/mL CPT to allow entry into S phase. Samples were collected at indicated time points. Cells were disrupted by glass bead beating in lysis buffer, followed by centrifugation at 20,000 g for 15 min to obtain whole-cell extract. The lysis buffer consisted of 25 mM K-HEPES (pH 7.6), 100 mM NaCl, 100 mM K-glutamate, 5 mM $Mg(OAc)_2$, 0.02% NP40, and 0.5% Triton X-100 supplemented by protease inhibitor cocktail (Sigma P8215) and Complete Ultra EDTA-free protease inhibitor (Roche 11836145001). The activated form of Mec1 was enriched by immunoprecipitating myc-tagged Ddc2 using Protein A beads and an anti-Myc antibody (Thermo Fisher 9E10) for 2–4 h at 4°C. Beads were washed five to six times with lysis buffer, and proteins were eluted using Laemmli buffer (65 mM Tris-HCl at pH 6.8, 2% SDS, 5% 2-mercaptoethanol, 10% glycerol, 0.025% bromophenol blue). After boiling for 5 min, eluted proteins were loaded onto NuPAGE™ 3–8% Tris-acetate gels for SDS-PAGE and subsequent immunoblotting analyses.

Immunoblotting analysis and antibodies. After SDS-PAGE, proteins were transferred to a 0.2-µm nitrocellulose membrane (GE, #G5678144) for immunoblotting. Pgk1 was used as a loading control. Antibodies used were anti-myc (Thermo, Fisher 9E10). anti-Srs2 (Santa Cruz,

yC-18), anti-Pgk1 (Invitrogen, 22C5D8), F9 (a kind gift from Marco Foiani and Daniele Piccini, The FIRC Institute of Molecular Oncology, Milan, Italy) (Pellicioli *et al.*, 2001), anti-Rad9 (a kind gift from John Petrini, MSKCC, NY, USA) (Usui *et al*, 2009), anti-Mec1-S1964-p (a kind gift from James E. Haber, Brandeis University, MA, USA) (Memisoglu *et al.*, 2019). Validation of antibodies is provided either by the manufacturers or in the cited references. Membranes were scanned with a Fujifilm LAS-3000 luminescent image analyzer, which has a linear dynamic range of 10^4. The signal intensities of non-saturated bands were measured using ImageJ software. For graphs, data are shown as mean and SD. Statistical differences were determined using two-sided Student's t tests.

Acknowledgments. We thank Drs. James Haber, Marco Foiani, Daniele Piccini, John Petrini for sharing antibodies, and Tzippora Chwat-Edelstein for critical reading of the manuscript. X.Z. is supported by National Institute of General Medical Sciences (NIGMS) grants R35GM145260.

Author contributions: All authors were involved in research design and data analyses, J. F., N. D., T. Y., and V. Y. performed research. J. F. and X.Z. wrote the paper with all authors' input.

Competing interest statement: The authors declare no competing interests.

Figure Legends.

Figure 1. Regulatory features of Srs2 and corresponding mutants.

(A) Schematic of Srs2 protein domains, regulatory features, and mutations affecting each of its features. Cdk1 phosphorylation sites depicted here include T604, S698, S879, S893, S938, S950, and S965 (Chiolo *et al.*, 2005). Potential Mec1 phosphorylation sites include S890 and S933 (Albuquerque *et al.*, 2015; Faca *et al.*, 2020). Sumoylation sites mapped previously include K1081, K1089, and K1142 (Saponaro *et al.*, 2010). Protein-interaction domains or motifs include the Rad51 binding domain (BD), PCNA Interaction Motif (PIM), and SUMO Interaction Motif (SIM) (Colavito *et al.*, 2009; Kolesar *et al.*, 2016; Kolesar *et al.*, 2012). The residues for these domains are indicated. Mutant alleles disabling each of these features are included in the parentheses.

(B) Mutations affecting Srs2 features do not affect Srs2 protein level. Protein extracts were prepared from asynchronous cells. Srs2 was examined using anti-Srs2 antibody by immunoblotting. Srs2 levels in each mutant were first normalized to the Pgk1 loading control and then to those in wild-type cells. Mean of two biological isolates per genotype is graphed with error bars representing standard deviation (SD).

Figure 2. Srs2 PCNA binding and sumoylation are involved in suppressing *rfa1* mutants

(A) Schematic to show that Srs2's roles in checkpoint dampening (anti-checkpoint for simplicity) and DNA repair both contribute to genotoxin resistance.

(B) Schematic to highlight the mutual suppression between *srs2*Δ and *rfa1* mutants and the underlying effects on the RPA-ssDNA levels in cells.

(C) *srs2-ΔPIM* and *-3KR* suppress *rfa1-zm2* sensitivity to CPT. A 10-fold serial dilution of cells of the indicated genotypes were spotted and growth was assessed after incubation at 30°C for 40 hours unless otherwise noted.

(D) Several *srs2* mutants did not suppress *rfa1-zm2* sensitivity to CPT. Experiments were performed as in panel 2C.

(E) *srs2-ΔPIM* and *-3KR* suppress *rfa1-t33* sensitivity to CPT. Top: schematic of the Rfa1 protein domains and *rfa1* mutant alleles. Bottom: *srs2-ΔPIM* and *-3KR* improved *CPT* sensitivity of *rfa1-t33* cells. Experiments were performed as in panel 2C.

Figure 3. *srs2-ΔPIM* and *-3KR* correct checkpoint abnormalities in *rfa1-zm2* cells.

(A) A table summarizing DDC levels observed in *rfa1-zm2*, *srs2* null or partially defective mutants, and their combined mutants in this work and in a previous study (Dhingra *et al.*, 2021) and interpretations.

(B) *srs2-ΔPIM* and *-3KR* reduce the levels of phosphorylated Rad53 in *rfa1-zm2* cells. Protein extracts were examined after G1 cells were released into cycling in the presence of 16 ug/ml CPT for 2 hours. Phosphorylated Rad53 (active form) was detected by the F9 antibody by immunoblotting. Phosphorylated Rad53 signals in each indicated strain were compared to the Pgk1 loading control and normalized to those of *rfa1-zm2*. Two biological isolates per genotype were examined in two technical repeats and results are graphed with error bars representing SD. Statistical analysis was performed using pairwise Student's t-test. *, p <0.05; ***, p <0.001; ****, p <0.0001.

(C) *srs2-ΔPIM* and *-3KR* allow better G1 entry of *rfa1-zm2* cells. Experiments were performed as in panel A and samples were collected at indicated time points. FACS profiles of the samples are shown at the top and percentages of G1 cells after 2 hours of CPT treatment (CPT 2 h) are plotted at the bottom. Two biological isolates per genotype were examined in two technique repeats and results are graphed with error bars representing SD. Statistical analysis was performed using pairwise Student's t-test. *, p <0.05; **, p <0.01.

Figure 4. *srs2-ΔPIM* and *slx4^{RIM}* are additively defective in DDC down-regulation.

(A) The *srs2-ΔPIMΔ slx4^{RIM}* double mutant shows stronger CPT sensitivity than either single mutant. Experiments are performed as in Figure 2C.

(B) *srs2-ΔPIM* and *slx4^{RIM}* are additive for increasing the level of phosphorylated Rad53 when cells are treated with CPT. Experiments were conducted and signals are quantified as those described in Figure 3B. Results from three biological isolates per genotype are graphed with error bars representing SD. Statistical analysis was performed using pairwise Student's t-test. *, p <0.05; **, p <0.01.

(C) *srs2-ΔPIM* and *slx4^{RIM}* are additive for reducing cells exiting from G2/M arrest at 2 hours post CPT treatment. Experiments were conducted and signals are quantified as those described in Figure 3C. Results from three biological isolates per genotype are graphed with error bars representing SD. Statistical analysis was performed using pairwise Student's t-test. *, p <0.05; **, p <0.01.

Figure 5. Srs2 sumoylation depends on Srs2 PIM motif and the Mec1 kinase

(A) Srs2 sumoylation level is reduced in *srs2-ΔPIM* cells. Samples were collected after CPT treatment as in Figure 3A and sumoylated proteins were enriched as described in the text and methods. Sumoylated form of Srs2 (Srs2-Su) migrated slower than unmodified Srs2 on gel and both were detected using anti-Srs2 antibody in immunoblotting. Equal loading is indicated by Ponceau-S stain (Stain). The levels of sumoylated Srs2 relative to those of unmodified Srs2 were normalized to wild-type cells and plotted. Two biological isolates per genotype were examined in two technique repeats and results are graphed with error bars representing SD. Statistical analysis was performed using pairwise Student's t-test. ns, not significant; *, p <0.05.

(B) Srs2 sumoylation level during CPT treatment. Samples were collected as described in Figure 3B. Experiments were conducted, and immunoblotting data is presented as those in

panel A. Time 0 samples are G1 cells before CPT treatment. FACS analysis at corresponding time points are included below the plot.

(C) Rad9 phosphorylation level during CPT treatment. Samples used in panel B were examined for Rad9 phosphorylation using an anti-Rad9 antibody. Unmodified and phosphorylated (Rad9-p) Rad9 forms are indicated. FACS analysis at corresponding time points are indicated below blots.

(D) Quantification of Srs2 sumoylation and Rad9 phosphorylation level changes during CPT treatment. Srs2 sumoylation signals were normalized based on unmodified form. Values at each timepoint were relative to that of G1 sample (Time 0) before CPT treatment, and fold changes were indicated on left y-axis. Rad9 signals were normalized to non-modified form and percentage of phosphorylated form were indicated on right y-axis. Results from three biological isolates per genotype are graphed.

(E) Mec1 is required for Srs2 sumoylation. Experiments were performed and data are presented as in panel A.

Figure 6. Mec1 and RPA phosphorylation did not link to Srs2 anti-checkpoint function.

(A) Mec1 autophosphorylation at S1964 during CPT treatment. Samples were collected as described in Figure 3B. Ddc2-myc was immunoprecipitated and the associated Mec1 was co-purified. The anti-Mec1-S1964-p antibody detected the phosphorylated form of Mec1 and a non-specific band (*). Quantification below the blot was based on results from two biological isolates.

(B) *mec1-S1964A* did not rescue *rfa1-zm2* sensitivity toward CPT. Experiments were performed as in Figure 2C.

(C) Examination of the *rfa1-S178A* and -*S178D* mutants. Top: schematic of the Rfa1 protein domains and position of Ser178. ssDNA binding domain (DBD) A-C are shown. Bottom, *rfa1-S178A* and -*S178D* had no effect on *srs2*Δ's sensitivity to CPT. Experiments were performed as in Figure 2C.

(D) Examination of the *rfa2-3SA* and -*3SD* mutants. Top, schematic of the Rfa2 protein domains and position of Ser122, Ser187 and Ser189 mutated in *rfa2-3SA* and -*3SD*. ssDNA binding domain (DBD)-D is indicated. Bottom, *rfa2-3SA* has no effect on *srs2*Δ's sensitivity toward CPT while *rfa2-3SD* showed additive effect. Experiments were performed as in Figure 2C.

Figure 7. A working model for the regulation of Srs2-mediated checkpoint dampening.
RPA-coated ssDNA regions generated from multiple DNA metabolic processes include those without proximal PCNA, such as ssDNA within R-loops and negatively supercoiled regions, and those with proximal PCNA, such as ssDNA gaps associated with perturbed DNA replication or repair. In latter situations, the resultant RPA-ssDNA can recruit the Mec1/Ddc2 kinase complex. Mec1 is subsequently activated by other DDC proteins, such as the 9-1-1 complex that demarcates the 5' end junctions adjacent to ssDNA regions (not drawn). After DDC is activated for a prolonged period, Srs2 recruited to PCNA that demarcates the 3' end junction flanking the ssDNA regions can be sumoylated. Srs2 sumoylation level increases as Mec1 activation heightens and can result in more efficient RPA removal, leading to Mec1 downregulation.

Fig. 1

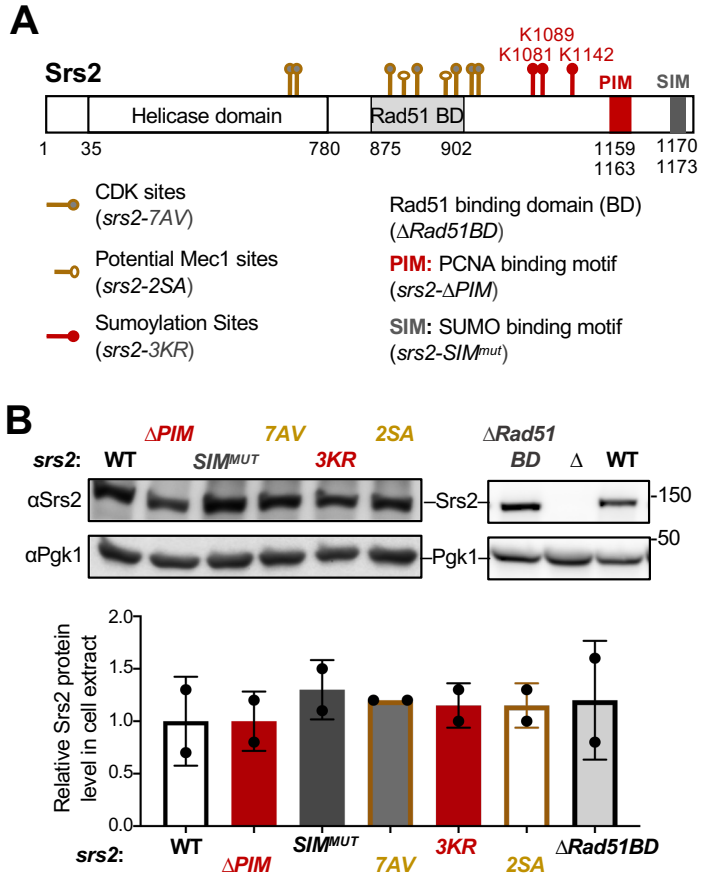
A
Srs2
K1089
K1081 K1142
PIM
SIM
Helicase domain
Rad51 BD
1
35
780
875
902
1159
1163
1170
1173
CDK sites
(srs2-7AV)
Potential Mec1 sites
(srs2-2SA)
Sumoylation Sites
(srs2-3KR)
Rad51 binding domain (BD)
(ΔRad51BD)
PIM: PCNA binding motif
(srs2-ΔPIM)
SIM: SUMO binding motif
(srs2-SIMmut)
B
srs2:
WT
ΔPIM
SIMMUT
7AV
3KR
2SA
ΔRad51 BD
Δ
WT
αSrs2
αPgk1
Srs2
Pgk1
150
50
Relative Srs2 protein level in cell extract
2.0
1.5
1.0
0.5
0.0
srs2:
WT
ΔPIM
SIMMUT
7AV
3KR
2SA
ΔRad51BD

Fig. 2

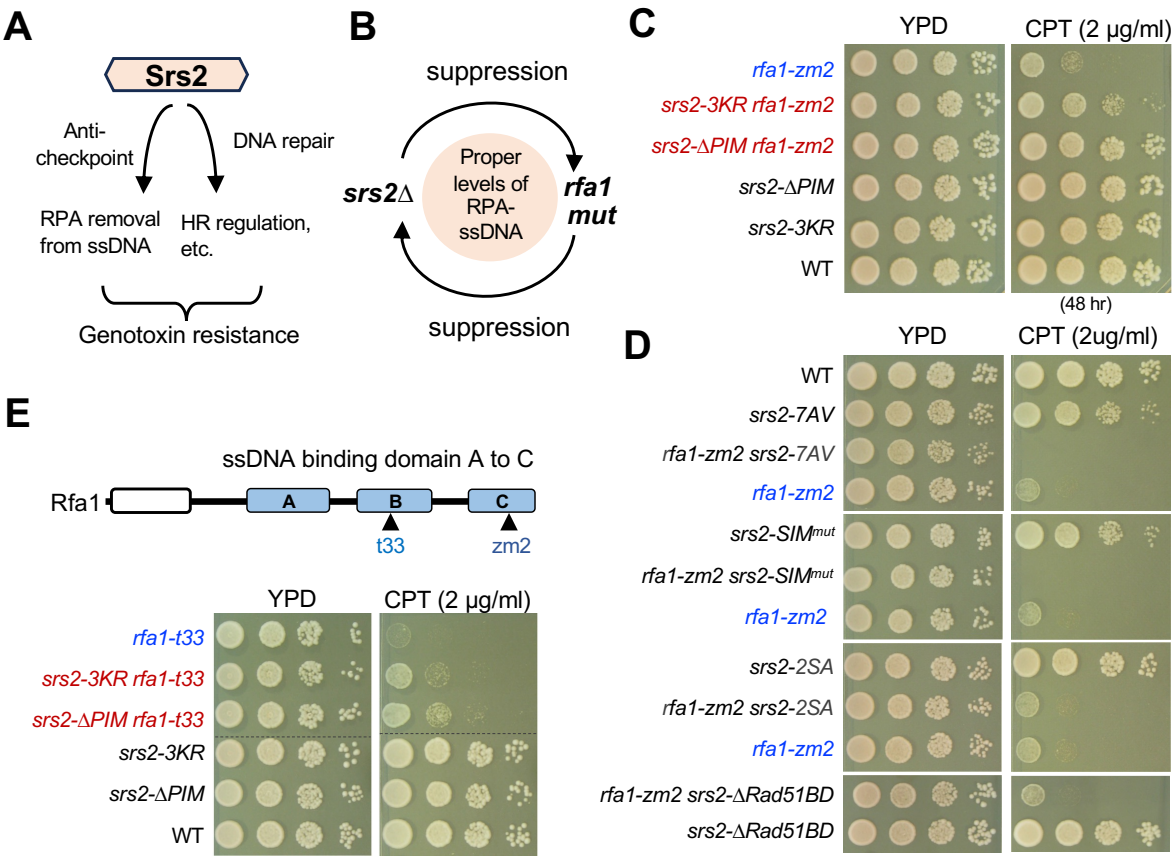
A
Srs2
Anti-checkpoint
DNA repair
RPA removal from ssDNA
HR regulation, etc.
Genotoxin resistance
B
suppression
srs2Δ
Proper levels of RPA-ssDNA
rfa1 mut
suppression
C
YPD
CPT (2 μg/ml)
rfa1-zm2
srs2-3KR rfa1-zm2
srs2-ΔPIM rfa1-zm2
srs2-ΔPIM
srs2-3KR
WT
(48 hr)
D
YPD
CPT (2ug/ml)
WT
srs2-7AV
rfa1-zm2 srs2-7AV
rfa1-zm2
srs2-SIMmut
rfa1-zm2 srs2-SIMmut
rfa1-zm2
srs2-2SA
rfa1-zm2 srs2-2SA
rfa1-zm2
rfa1-zm2 srs2-ΔRad51BD
srs2-ΔRad51BD
E
ssDNA binding domain A to C
Rfa1
A
B
C
t33
zm2
YPD
CPT (2 μg/ml)
rfa1-t33
srs2-3KR rfa1-t33
srs2-ΔPIM rfa1-t33
srs2-3KR
srs2-ΔPIM
WT

Fig. 3

A

Mutants	Checkpoint levels	Interpretations
rfa1-zm2	Increased	Suboptimal RPA levels on DNA lead to increased DNA lesions and checkpoint activiation
rfa1-zm2 *srs2Δ (srs2-ΔPIM or srs2-3KR)*	Normal	RPA levels on DNA and checkpoint levels are restored compared with *rfa1-zm2*
srs2-ΔPIM or srs2-3KR	Normal	Mild-defects of partially defective *srs2* alleles is masked by other checkpoint dampening proteins

B

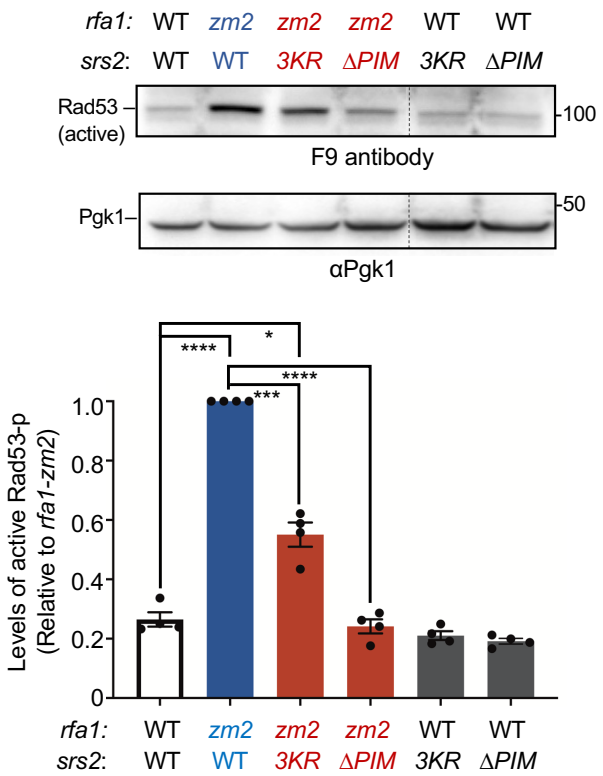

C

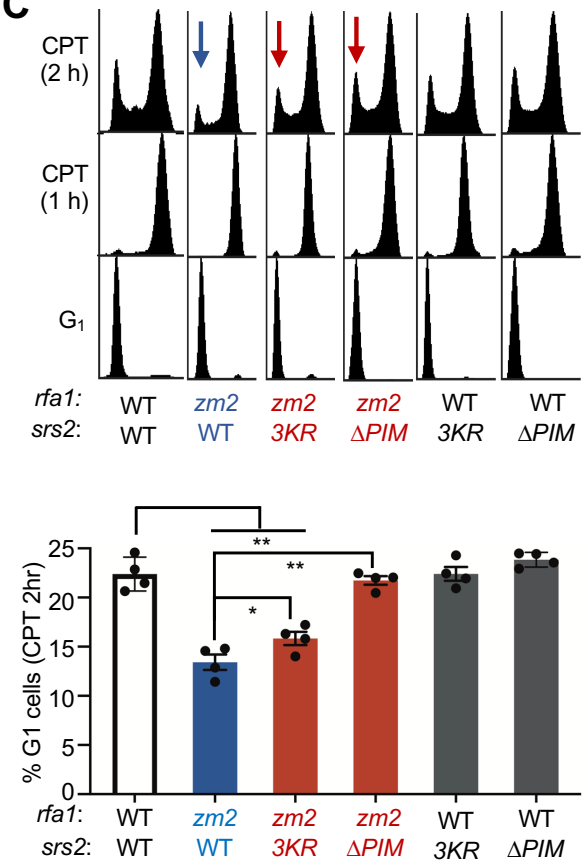

Fig. 4

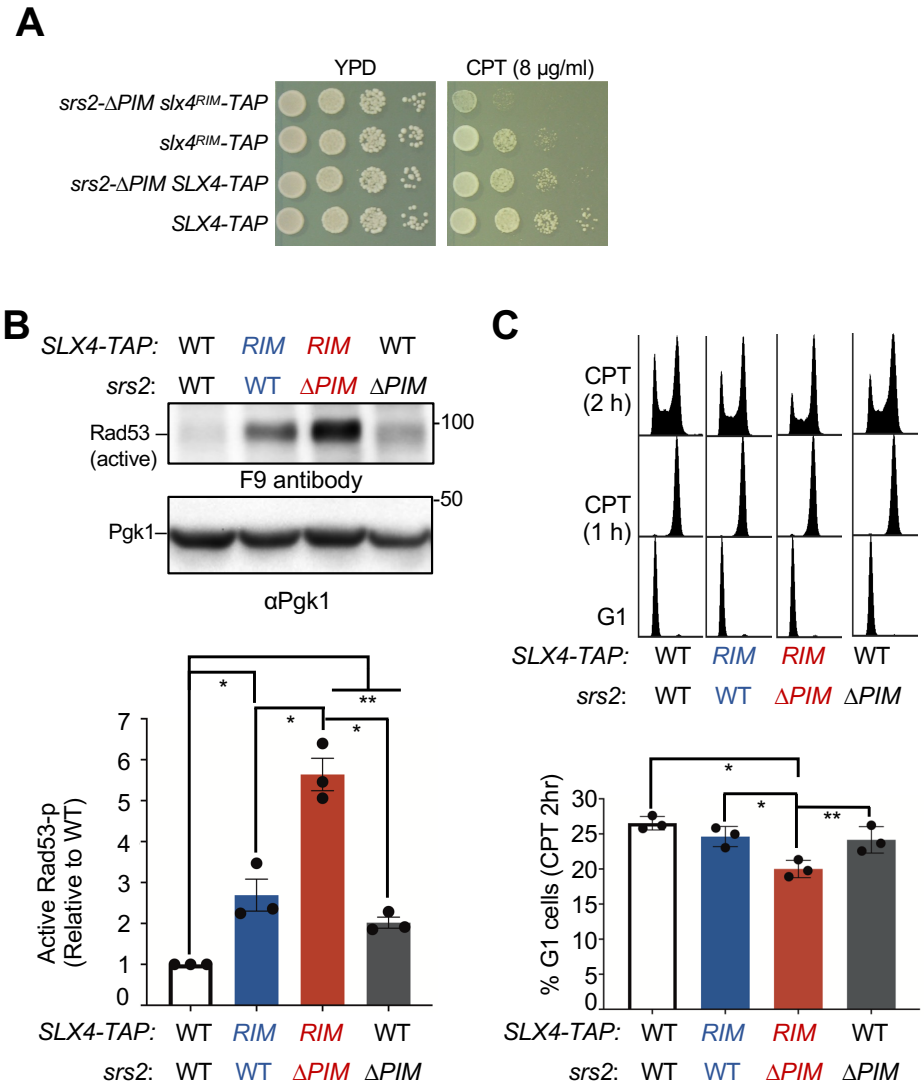
A
YPD
CPT (8 μg/ml)
srs2-ΔPIM slx4RIM-TAP
slx4RIM-TAP
srs2-ΔPIM SLX4-TAP
SLX4-TAP
B
SLX4-TAP: WT RIM RIM WT
srs2: WT WT ΔPIM ΔPIM
Rad53 (active)
100
F9 antibody
50
Pgk1
αPgk1
Active Rad53-p (Relative to WT)
0
1
2
3
4
5
6
7
*
*
*
**
SLX4-TAP: WT RIM RIM WT
srs2: WT WT ΔPIM ΔPIM
C
CPT (2 h)
CPT (1 h)
G1
SLX4-TAP: WT RIM RIM WT
srs2: WT WT ΔPIM ΔPIM
% G1 cells (CPT 2hr)
0
5
10
15
20
25
30
*
*
**
SLX4-TAP: WT RIM RIM WT
srs2: WT WT ΔPIM ΔPIM

Fig. 5

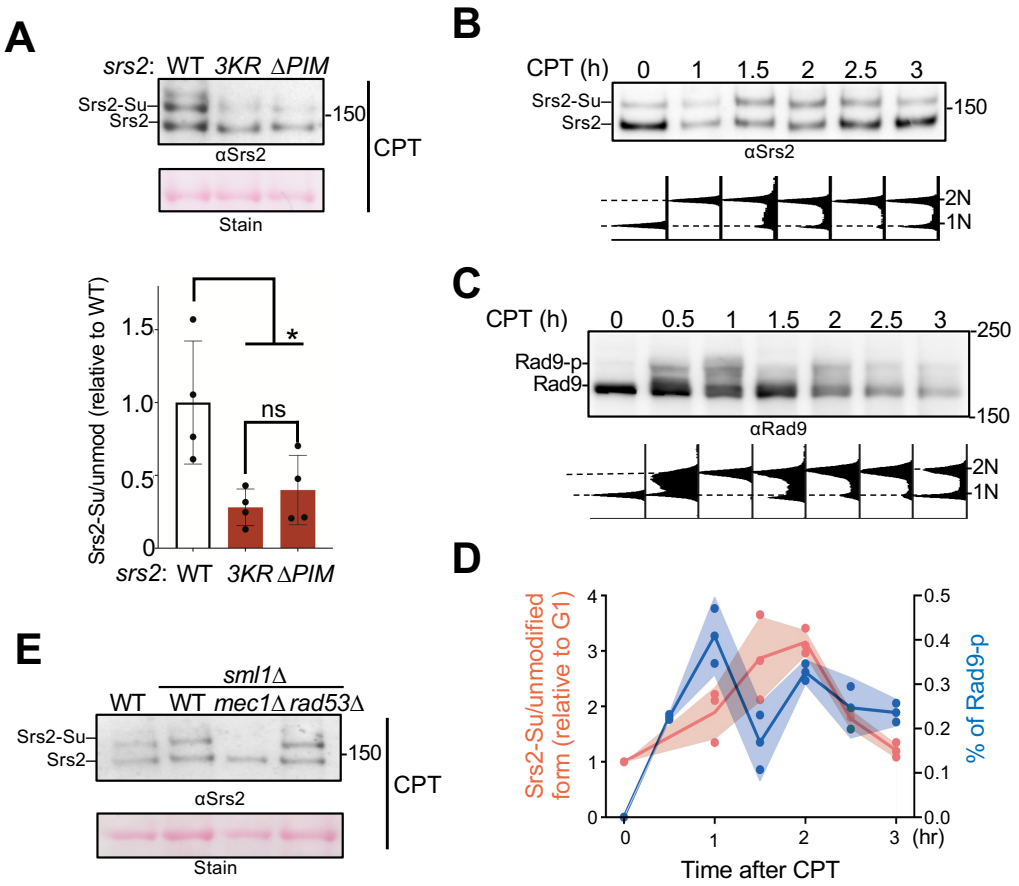
A
srs2: WT 3KR ΔPIM
Srs2-Su
Srs2
150
αSrs2
CPT
Stain
Srs2-Su/unmod (relative to WT)
1.5
1.0
0.5
0
*
ns
srs2: WT 3KR ΔPIM
B
CPT (h) 0 1 1.5 2 2.5 3
Srs2-Su
Srs2
150
αSrs2
2N
1N
C
CPT (h) 0 0.5 1 1.5 2 2.5 3
250
Rad9-p
Rad9
150
αRad9
2N
1N
D
Srs2-Su/unmodified form (relative to G1)
% of Rad9-p
Time after CPT
(hr)
E
sml1Δ
WT WT mec1Δ rad53Δ
Srs2-Su
Srs2
150
αSrs2
CPT
Stain

Fig. 6

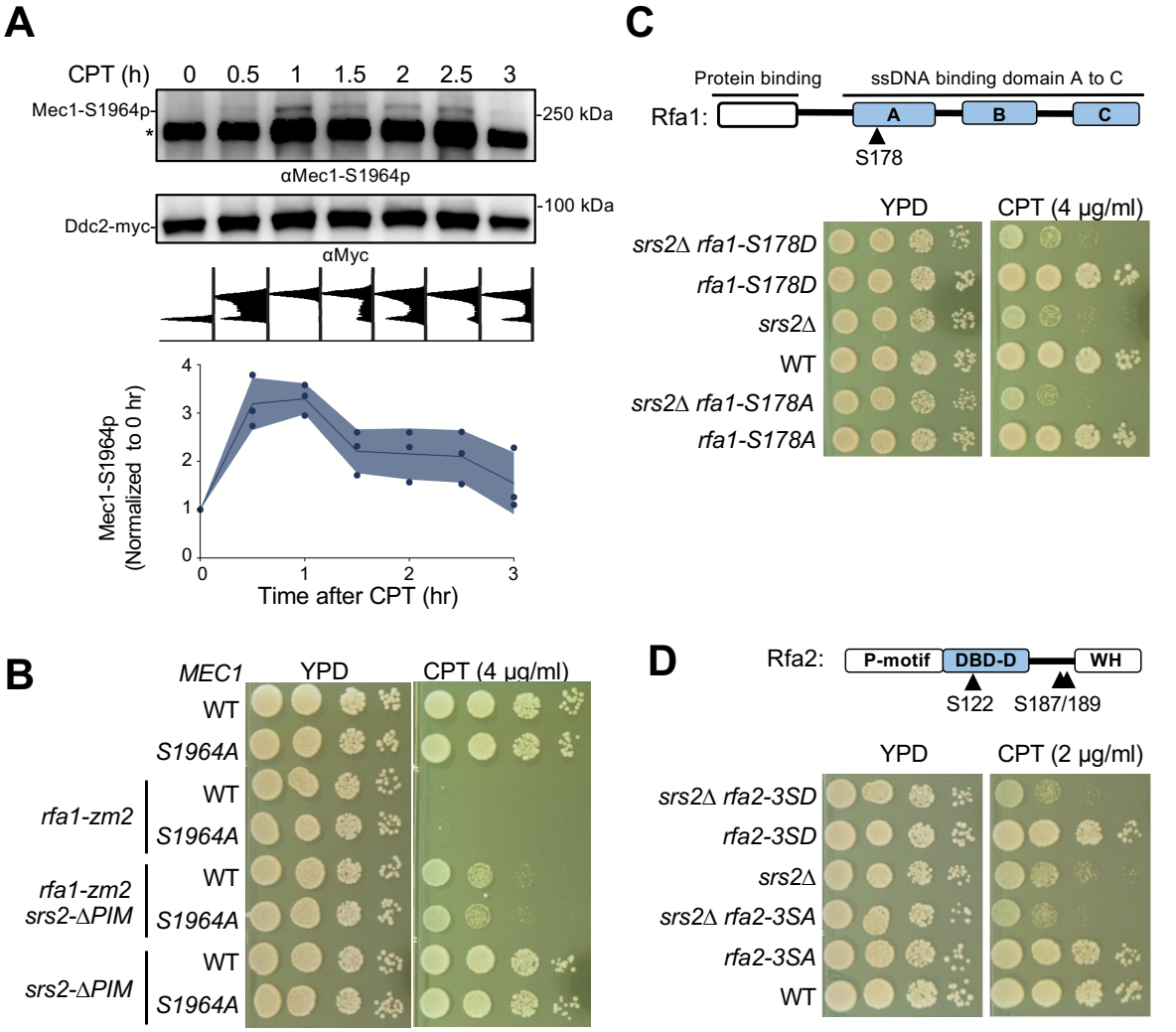
A
CPT (h) 0 0.5 1 1.5 2 2.5 3
Mec1-S1964p
*
250 kDa
αMec1-S1964p
Ddc2-myc
100 kDa
αMyc
Mec1-S1964p (Normalized to 0 hr)
Time after CPT (hr)
C
Protein binding
ssDNA binding domain A to C
Rfa1:
A
B
C
S178
YPD
CPT (4 μg/ml)
srs2Δ rfa1-S178D
rfa1-S178D
srs2Δ
WT
srs2Δ rfa1-S178A
rfa1-S178A
B
MEC1
YPD
CPT (4 μg/ml)
WT
S1964A
rfa1-zm2
rfa1-zm2 srs2-ΔPIM
srs2-ΔPIM
D
Rfa2:
P-motif
DBD-D
WH
S122
S187/189
YPD
CPT (2 μg/ml)
srs2Δ rfa2-3SD
rfa2-3SD
srs2Δ
srs2Δ rfa2-3SA
rfa2-3SA
WT

Fig. 7

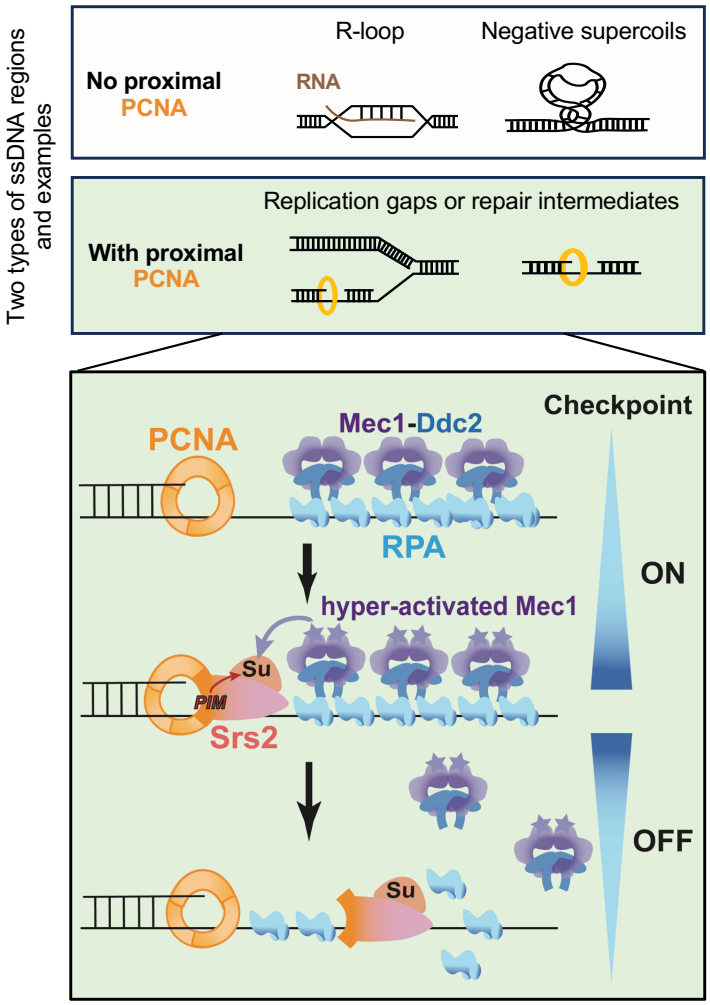
Two types of ssDNA regions and examples
No proximal PCNA
R-loop
RNA
Negative supercoils
With proximal PCNA
Replication gaps or repair intermediates
Checkpoint
PCNA
Mec1-Ddc2
RPA
ON
hyper-activated Mec1
Su
PIM
Srs2
OFF
Su

Reference:

Albuquerque CP, Yeung E, Ma S, Fu T, Corbett KD, Zhou H (2015) A chemical and enzymatic approach to study site-specific sumoylation. *PLoS ONE* 10: e0143810.

Antony E, Tomko EJ, Xiao Q, Krejci L, Lohman TM, Ellenberger T (2009) Srs2 disassembles Rad51 filaments by a protein-protein interaction triggering ATP turnover and dissociation of Rad51 from DNA. *Mol Cell* 35: 105-115.

Bronstein A, Bramson S, Shemesh K, Liefshitz B, Kupiec M (2018) Tight regulation of Srs2 helicase activity is crucial for proper functioning of DNA repair mechanisms. *G3* 8: 1615-1626.

Chen SH, Albuquerque CP, Liang J, Suhandynata RT, Zhou H (2010) A proteome-wide analysis of kinase-substrate network in the DNA damage response. *J Biol Chem* 285: 12803-12812.

Chiolo I, Carotenuto W, Maffioletti G, Petrini JH, Foiani M, Liberi G (2005) Srs2 and Sgs1 DNA helicases associate with Mre11 in different subcomplexes following checkpoint activation and CDK1-mediated Srs2 phosphorylation. *Mol Cell Biol* 25: 5738-5751.

Chung I, Zhao X (2015) DNA break-induced sumoylation is enabled by collaboration between a SUMO ligase and the ssDNA-binding complex RPA. *Genes Dev* 29: 1593-1598.

Colavito S, Macris-Kiss M, Seong C, Gleeson O, Greene EC, Klein HL, Krejci L, Sung P (2009) Functional significance of the Rad51-Srs2 complex in Rad51 presynaptic filament disruption. *Nucleic Acids Res* 37: 6754-6764.

Cremona CA, Sarangi P, Yang Y, Hang LE, Rahman S, Zhao X (2012) Extensive DNA damage-induced sumoylation contributes to replication and repair and acts in addition to the Mec1 checkpoint. *Mol Cell* 45: 422-432.

Deng SK, Gibb B, de Almeida MJ, Greene EC, Symington LS (2014) RPA antagonizes microhomology-mediated repair of DNA double-strand breaks. *Nat Struct Mol Biol* 21: 405-412.

Dhingra N, Kuppa S, Wei L, Pokhrel N, Baburyan S, Meng X, Antony E, Zhao X (2021) The Srs2 helicase dampens DNA damage checkpoint by recycling RPA from chromatin. *Proc Natl Acad Sci U S A* 118: e2020185118.

DiCarlo JE, Norville JE, Mali P, Rios X, Aach J, Church GM (2013) Genome engineering in Saccharomyces cerevisiae using CRISPR-Cas systems. *Nucleic Acids Res* 41: 4336-4343.

Elledge SJ (1996) Cell cycle checkpoints: preventing an identity crisis. *Science* 274: 1664-1672.

Enoch T, Carr AM, Nurse P (1992) Fission yeast genes involved in coupling mitosis to completion of DNA replication. *Genes Dev* 6: 2035-2046.

Faca VM, Sanford EJ, Tieu J, Comstock W, Gupta S, Marshall S, Yu H, Smolka MB (2020) Maximized quantitative phosphoproteomics allows high confidence dissection of the DNA damage signaling network. *Sci Rep* 10: 18056.

Fan J, Pavletich NP (2012) Structure and conformational change of a Replication Protein A heterotrimer bound to ssDNA. *Genes Dev* 26: 2337-2347.

Fan L, Zhang W, Rybchuk J, Luo Y, Xiao W (2023) Genetic dissection of budding yeast PCNA mutations responsible for the regulated recruitment of Srs2 helicase. *mBio* 14: e0031523.

Fiorani S, Mimun G, Caleca L, Piccini D, Pellicioli A (2008) Characterization of the activation domain of the Rad53 checkpoint kinase. *Cell Cycle* 7: 493-499.

Foiani M, Pellicioli A, Lopes M, Lucca C, Ferrari M, Liberi G, Muzi Falconi M, Plevani P (2000) DNA damage checkpoints and DNA replication controls in *Saccharomyces cerevisiae*. *Mutat Res* 451: 187-196.

Harrison JC, Haber JE (2006) Surviving the breakup: the DNA damage checkpoint. *Annu Rev Genet* 40: 209-235.

Hartwell LH, Weinert TA (1989) Checkpoints: controls that ensure the order of cell cycle events. *Science* 246: 629-634.

Hormeno S, Wilkinson OJ, Aicart-Ramos C, Kuppa S, Antony E, Dillingham MS, Moreno-Herrero F (2022) Human HELB is a processive motor protein that catalyzes RPA clearance from single-stranded DNA. *Proc Natl Acad Sci U S A* 119: e2112376119.

Jenkins T, Northall SJ, Ptchelkine D, Lever R, Cubbon A, Betts H, Taresco V, Cooper CDO, McHugh PJ, Soultanas P, Bolt EL (2021) The HelQ human DNA repair helicase utilizes a PWI-like domain for DNA loading through interaction with RPA, triggering DNA unwinding by the HelQ helicase core. *NAR Cancer* 3: zcaa043.

Kolesar P, Altmannova V, Silva S, Lisby M, Krejci L (2016) Pro-recombination role of Srs2 protein requires SUMO (Small Ubiquitin-like Modifier) but is independent of PCNA (Proliferating Cell Nuclear Antigen) interaction. *J Biol Chem* 291: 7594-7607.

Kolesar P, Sarangi P, Altmannova V, Zhao X, Krejci L (2012) Dual roles of the SUMO-interacting motif in the regulation of Srs2 sumoylation. *Nucleic Acids Res* 40: 7831-7843.

Krejci L, Van Komen S, Li Y, Villemain J, Reddy MS, Klein H, Ellenberger T, Sung P (2003) DNA helicase Srs2 disrupts the Rad51 presynaptic filament. *Nature* 423: 305-309.

Lanz MC, Dibitetto D, Smolka MB (2019) DNA damage kinase signaling: checkpoint and repair at 30 years. *EMBO J* 38: e101801.

Lanz MC, Yugandhar K, Gupta S, Sanford EJ, Faca VM, Vega S, Joiner AMN, Fromme JC, Yu H, Smolka MB (2021) In-depth and 3-dimensional exploration of the budding yeast phosphoproteome. *EMBO Rep* 22: e51121.

Li S, Xu Z, Xu J, Zuo L, Yu C, Zheng P, Gan H, Wang X, Li L, Sharma S *et al* (2018) Rtt105 functions as a chaperone for Replication Protein A to preserve genome stability. *EMBO J* 37: e99154.

Majka J, Binz SK, Wold MS, Burgers PM (2006) Replication Protein A directs loading of the DNA damage checkpoint clamp to 5'-DNA junctions. *J Biol Chem* 281: 27855-27861.

Marechal A, Zou L (2015) RPA-coated single-stranded DNA as a platform for post-translational modifications in the DNA damage response. *Cell Res* 25: 9-23.

Meir A, Raina VB, Rivera CE, Marie L, Symington LS, Greene EC (2023) The separation pin distinguishes the pro- and anti-recombinogenic functions of *Saccharomyces cerevisiae* Srs2. *Nat Commun* 14: 8144.

Memisoglu G, Lanz MC, Eapen VV, Jordan JM, Lee K, Smolka MB, Haber JE (2019) Mec1(ATR) autophosphorylation and Ddc2(ATRIP) phosphorylation regulates dna damage checkpoint signaling. *Cell Rep* 28: 1090-1102 e1093.

Menin L, Ursich S, Trovesi C, Zellweger R, Lopes M, Longhese MP, Clerici M (2018) Tel1/ATM prevents degradation of replication forks that reverse after topoisomerase poisoning. *EMBO Rep* 19: e45535.

Moldovan GL, Pfander B, Jentsch S (2007) PCNA, the maestro of the replication fork. *Cell* 129: 665-679.

Niu H, Klein HL (2017) Multifunctional roles of *Saccharomyces cerevisiae* Srs2 protein in replication, recombination and repair. *FEMS Yeast Res* 17: fow111.

Ohouo PY, Bastos de Oliveira FM, Almeida BS, Smolka MB (2010) DNA damage signaling recruits the Rtt107-Slx4 scaffolds via Dpb11 to mediate replication stress response. *Mol Cell* 39: 300-306.

Ohouo PY, Bastos de Oliveira FM, Liu Y, Ma CJ, Smolka MB (2013) DNA-repair scaffolds dampen checkpoint signalling by counteracting the adaptor Rad9. *Nature* 493: 120-124.

Paciotti V, Clerici M, Lucchini G, Longhese MP (2000) The checkpoint protein Ddc2, functionally related to *S. pombe* Rad26, interacts with Mec1 and is regulated by Mec1-dependent phosphorylation in budding yeast. *Genes Dev* 14: 2046-2059.

Papouli E, Chen S, Davies AA, Huttner D, Krejci L, Sung P, Ulrich HD (2005) Crosstalk between SUMO and ubiquitin on PCNA is mediated by recruitment of the helicase Srs2p. *Mol Cell* 19: 123-133.

Pellicioli A, Lee SE, Lucca C, Foiani M, Haber JE (2001) Regulation of *Saccharomyces* Rad53 checkpoint kinase during adaptation from DNA damage-induced G2/M arrest. *Mol Cell* 7: 293-300.

Pfander B, Moldovan GL, Sacher M, Hoege C, Jentsch S (2005) SUMO-modified PCNA recruits Srs2 to prevent recombination during S phase. *Nature* 436: 428-433.

Pommier Y, Nussenzweig A, Takeda S, Austin C (2022) Human topoisomerases and their roles in genome stability and organization. *Nat Rev Mol Cell Biol* 23: 407-427.

Psakhye I, Jentsch S (2012) Protein group modification and synergy in the SUMO pathway as exemplified in DNA repair. *Cell* 151: 807-820.

Redon C, Pilch DR, Rogakou EP, Orr AH, Lowndes NF, Bonner WM (2003) Yeast histone 2A serine 129 is essential for the efficient repair of checkpoint-blind DNA damage. *EMBO Rep* 4: 678-684.

Regan-Mochrie G, Hoggard T, Bhagwat N, Lynch G, Hunter N, Remus D, Fox CA, Zhao X (2022) Yeast ORC sumoylation status fine-tunes origin licensing. *Genes Dev* 36: 807-821.

Sanchez Y, Bachant J, Wang H, Hu F, Liu D, Tetzlaff M, Elledge SJ (1999) Control of the DNA damage checkpoint by Chk1 and Rad53 protein kinases through distinct mechanisms. *Science* 286: 1166-1171.

Saponaro M, Callahan D, Zheng X, Krejci L, Haber JE, Klein HL, Liberi G (2010) Cdk1 targets Srs2 to complete synthesis-dependent strand annealing and to promote recombinational repair. *PLoS Genet* 6: e1000858.

Seeber A, Hegnauer AM, Hustedt N, Deshpande I, Poli J, Eglinger J, Pasero P, Gut H, Shinohara M, Hopfner KP *et al* (2016) RPA Mediates Recruitment of MRX to Forks and Double-Strand Breaks to Hold Sister Chromatids Together. *Mol Cell* 64: 951-966.

Shorrocks AK, Jones SE, Tsukada K, Morrow CA, Belblidia Z, Shen J, Vendrell I, Fischer R, Kessler BM, Blackford AN (2021) The Bloom syndrome complex senses RPA-coated single-stranded DNA to restart stalled replication forks. *Nat Commun* 12: 585.

Smith J, Rothstein R (1995) A mutation in the gene encoding the *Saccharomyces cerevisiae* single-stranded DNA-binding protein Rfa1 stimulates a RAD52-independent pathway for direct-repeat recombination. *Mol Cell Biol* 15: 1632-1641.

Sogo JM, Lopes M, Foiani M (2002) Fork reversal and ssDNA accumulation at stalled replication forks owing to checkpoint defects. *Science* 297: 599-602.

Sun Y, Saha S, Wang W, Saha LK, Huang SN, Pommier Y (2020) Excision repair of topoisomerase DNA-protein crosslinks (TOP-DPC). *DNA Repair* 89: 102837.

Tercero JA, Longhese MP, Diffley JFX (2003) A central role for DNA replication forks in checkpoint activation and response. *Mol Cell* 11: 1323-1336.

Ulrich HD, Davies AA (2009) In vivo detection and characterization of sumoylation targets in *Saccharomyces cerevisiae*. *Methods Mol Biol* 497: 81-103.

Umezu K, Sugawara N, Chen C, Haber JE, Kolodner RD (1998) Genetic analysis of yeast RPA1 reveals its multiple functions in DNA metabolism. *Genetics* 148: 989-1005.

Usui T, Foster SS, Petrini JH (2009) Maintenance of the DNA-damage checkpoint requires DNA-damage-induced mediator protein oligomerization. *Mol Cell* 33: 147-159.

Usui T, Ogawa H, Petrini JH (2001) A DNA damage response pathway controlled by Tel1 and the Mre11 complex. *Mol Cell* 7: 1255-1266.

Wan B, Wu J, Meng X, Lei M, Zhao X (2019) Molecular Basis for Control of Diverse Genome Stability Factors by the Multi-BRCT Scaffold Rtt107. *Mol Cell* 75: 238-251 e235.

Wang H, Liu D, Wang Y, Qin J, Elledge SJ (2001) Pds1 phosphorylation in response to DNA damage is essential for its DNA damage checkpoint function. *Genes Dev* 15: 1361-1372.

Waterman DP, Haber JE, Smolka MB (2020) Checkpoint responses to DNA double-strand breaks. *Annu Rev Biochem* 89: 103-133.

Zhao X, Blobel G (2005) A SUMO ligase is part of a nuclear multiprotein complex that affects DNA repair and chromosomal organization. *Proc Natl Acad Sci U S A* 102: 4777-4782.

Zhao X, Muller EG, Rothstein R (1998) A suppressor of two essential checkpoint genes identifies a novel protein that negatively affects dNTP pools. *Mol Cell* 2: 329-340.

Zhao X, Rothstein R (2002) The Dun1 checkpoint kinase phosphorylates and regulates the ribonucleotide reductase inhibitor Sml1. *Proc Natl Acad Sci U S A* 99: 3746-3751.

Zou L, Elledge SJ (2003) Sensing DNA damage through ATRIP recognition of RPA-ssDNA complexes. *Science* 300: 1542-1548.

Supplemental Materials

Figure S1. *srs2* mutants examined for CPT sensitivity and interactions with *rfa1* mutant.

(A) *srs2* mutants exhibit different levels of CPT sensitivity. *srs2-ΔPIM* showed slow growth on 8 µg/ml CPT. Sensitivity *srs2-SIM^{MUT}* toward CPT was seen at three CPT concentrations. *srs2-7AV* showed slow growth on media containing 4 and 8 µg/ml CPT. *srs2Δ* and *rfa1-zm2* are mutually suppressive for CPT sensitivity. Experiments are performed as in Figure 2C.

(B) *srs2-ΔPIM* confers better suppression of *rfa1-zm2's* CPT and MMS sensitivity than *srs2-3KR*. We note that mild suppression of *rfa1-zm2* by *srs2-3KR* was only seen at 0.03% MMS plates. Experiments are performed as in Figure 2C, and incubation times are noted. Dashed lines indicate the removal of superfluous rows.

(C) *srs2-ΔPIM* suppresses *rfa1-t33* sensitivity toward MMS. Dashed lines indicate the removal of superfluous rows.

Figure S2. Confirmation of Srs2 sumoylation and Mec1-S1964 phosphorylation.

(A) Detection of Srs2 sumoylation. Protein extracts from asynchronous cells were bound to Ni-NTA beads and the elutes were examined by immunoblotting using an anti-Srs2 antibody. Sumoylated Srs2 form was detected in wild-type cells expressing 8His-tagged SUMO (Smt3) but not in cells lacking this construct or in *srs2Δ* cells. Unmodified Srs2 showed unspecific Ni-NTA bead binding, thus being detectable in cells containing Srs2 regardless of the SUMO status.

(B) Detection of Mec1-S1964 phosphorylation. Cells were treated with CPT for 2 hours before immunoprecipitating Ddc2-myc was conducted. Ddc2 and the co-immunoprecipitated Mec1 were examined by immunoblotting. Phosphorylation of Ser1964 of the Mec1 protein was detected using the anti-Mec1-S1964-p antibody. This antibody also detected a non-specific band (*). Cells containing untagged Ddc2 or the *mec1-S1964A* mutation were used as controls.

Figure S3. Examination of Mec1-S964 phosphorylation.

(A) *mec1-S1964A* does not affect the CPT sensitivity of *srs2-3KR* or *srs2-3KR rfa1-zm2* cells. Experiments were performed as in Figure 2C.

(B) The effects of *mec1-S1964E* on the CPT sensitivity of *srs2-3KR* and *srs2-ΔPIM* cells with or without *rfa1-zm2*. Experiments were performed as in Figure 2C.

(C) *mec1-S1964A* or *-S1964E* does not affect Srs2 sumoylation. Experiments were performed as in Figure 4A. Mean values of three biological isolates per genotype are graphed, with error bars representing SD. Statistical analysis was performed using pairwise Student's t-test; no significance was found between values of wild-type and mutant strains.

Figure S4. *srs2-Y775A* improves *rfa1-zm2* mutant growth on CPT containing media.

The endogenous *SRS2* gene was deleted in cells, while the wild-type *SRS2* or the *srs2-Y775A* allele was integrated at the *HIS3* locus (Meir *et al.*, 2023). The control strain contains vector sequence integrated at the *HIS3* locus (Meir *et al.*, 2023). Experiments were performed as in Figure 2C.

Fig. S1

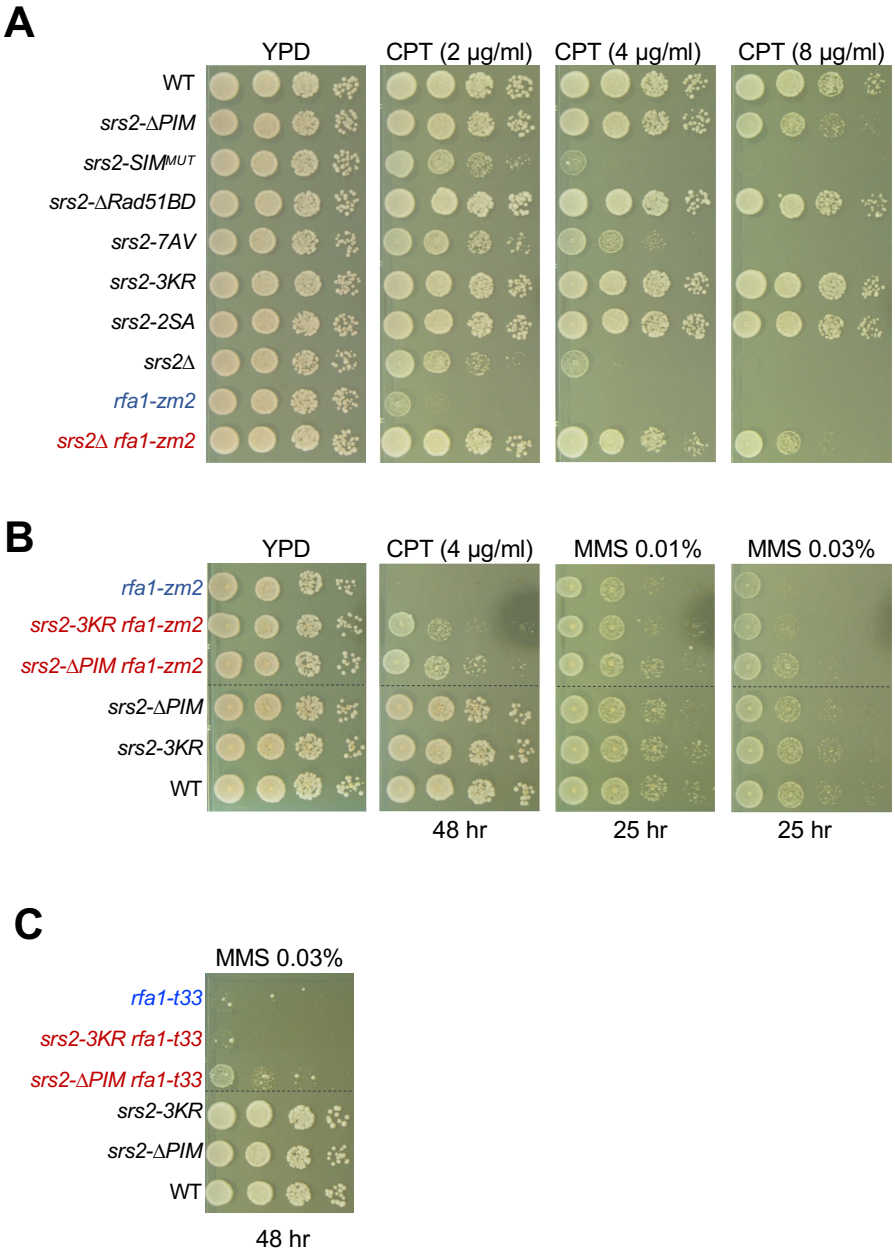
A
YPD
CPT (2 μg/ml)
CPT (4 μg/ml)
CPT (8 μg/ml)
WT
srs2-ΔPIM
srs2-SIMMUT
srs2-ΔRad51BD
srs2-7AV
srs2-3KR
srs2-2SA
srs2Δ
rfa1-zm2
srs2Δ rfa1-zm2
B
YPD
CPT (4 μg/ml)
MMS 0.01%
MMS 0.03%
rfa1-zm2
srs2-3KR rfa1-zm2
srs2-ΔPIM rfa1-zm2
srs2-ΔPIM
srs2-3KR
WT
48 hr
25 hr
25 hr
C
MMS 0.03%
rfa1-t33
srs2-3KR rfa1-t33
srs2-ΔPIM rfa1-t33
srs2-3KR
srs2-ΔPIM
WT
48 hr

Fig. S2

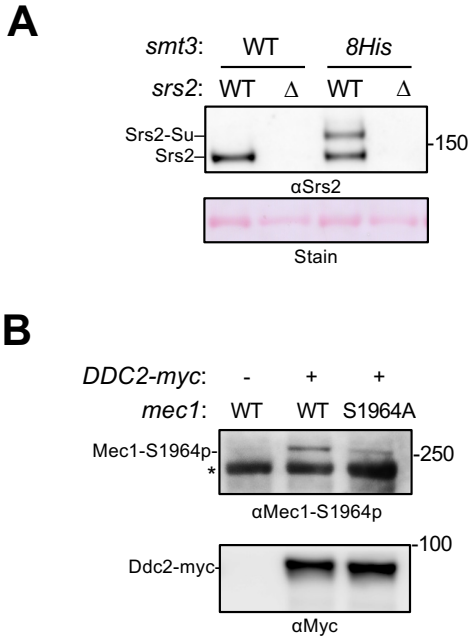
A
smt3: WT 8His
srs2: WT Δ WT Δ
Srs2-Su
Srs2
150
αSrs2
Stain
B
DDC2-myc: - + +
mec1: WT WT S1964A
Mec1-S1964p
*
250
αMec1-S1964p
100
Ddc2-myc
αMyc

Fig. S3

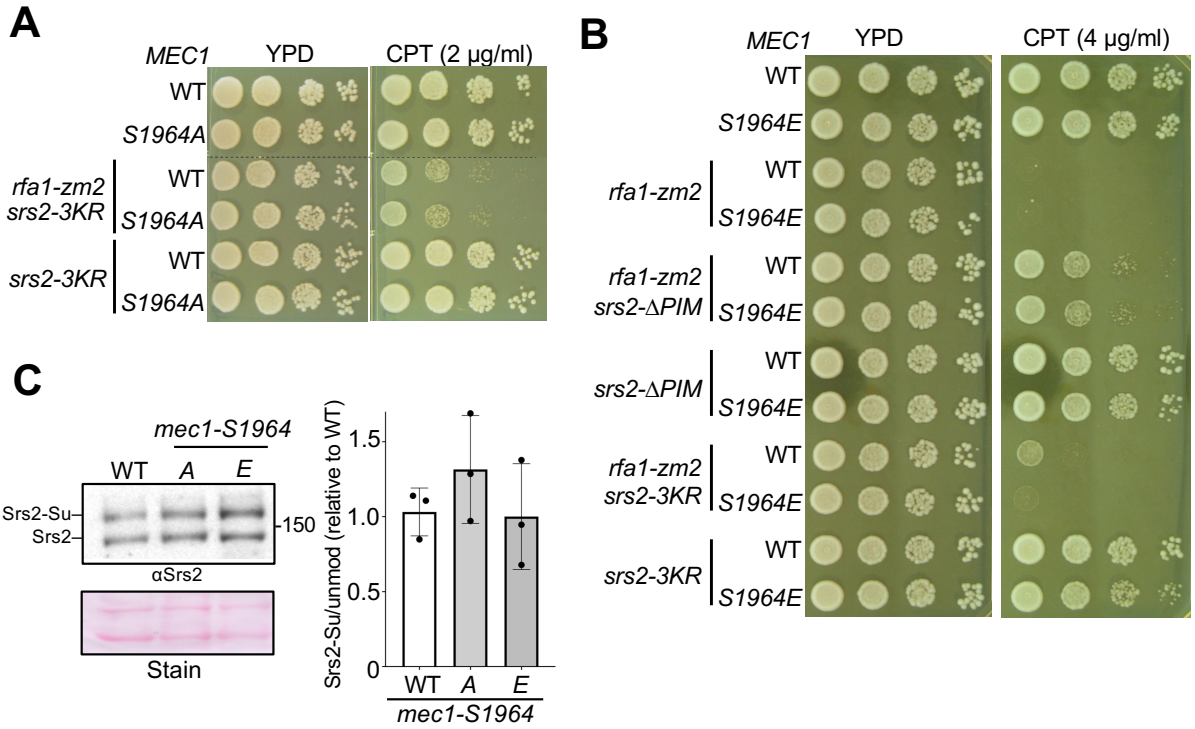
A
MEC1
YPD
CPT (2 μg/ml)
WT
S1964A
rfa1-zm2
srs2-3KR
WT
S1964A
srs2-3KR
WT
S1964A
B
MEC1
YPD
CPT (4 μg/ml)
WT
S1964E
rfa1-zm2
WT
S1964E
rfa1-zm2
srs2-ΔPIM
WT
S1964E
srs2-ΔPIM
WT
S1964E
rfa1-zm2
srs2-3KR
WT
S1964E
srs2-3KR
WT
S1964E
C
mec1-S1964
WT
A
E
Srs2-Su
Srs2
150
αSrs2
Stain
Srs2-Su/unmod (relative to WT)
1.5
1.0
0.5
0
WT
A
E
mec1-S1964

Fig. S4

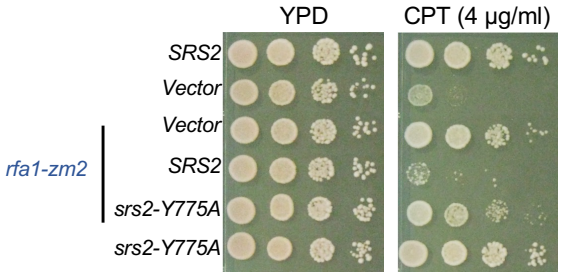

Endogenous *SRS2* deleted in all cells.

Table S1: Strains Sources.

All strains are derived from W1588-4C, a *RAD5* derivative of W303 (*MATa ade2-1 can1-100 ura3-1 his3-11,15, leu2-3, 112 trp1-1 rad5-535*). Only one strain is listed per each genotype, but at least two independent isolates of each genotype were used in the experiments.

Strain	Genotype	Source	Used In Figures
G16	Wild-type W303 *RAD5* strain	Lab collection	1B, 2C-E, 3B-C, 5C, 6B-D, S1-3
X8047-14B	*srs2Δ*	(Dhingra *et al.*, 2021)	6C-D, S1A, S2A
X8665-12-22D	*MATa srs2-ΔPIM*	This study	1B, 2C, 3B-C, 6B, S1A-C
X8198-15B	*srs2-SIM^{MUT}*	This study	1B, 2D, S1A
G1114	*MATa srs2-7AV::HIS3*	(Saponaro *et al.*, 2010)	1B, 2D, S1A
X8650-2-1D	*MATa srs2-3KR::NAT*	This study	1B, 2C, 3B-C, S1A-C
X8659-14A	*MATa srs2-2SA*	This study	1B, 2D, S1A
G854	*MATα srs2-Δ(875-902)::HPH*	(Colavito *et al.*, 2009)	1B, 2D, S1A
X8047-1B	*MATα rfa1-zm2*	(Dhingra *et al.*, 2021)	2C, 2C-D, 3B-C, 6B, S1A-B, S3B
X8650-2C	*MATa srs2-3KR::NAT rfa1-zm2*	This study	2C, 3B-C, S1B, S3A-B
X8666-35-6A	*MATa srs2-ΔPIM rfa1-zm2*	This study	2C, 3B-C, 6B, S1B, S3B
X8210-2B	*MATa rfa1-t33*	(Dhingra *et al.*, 2021)	2E, S1C
X8745-2A	*MATa srs2-3KR::NAT rfa1-t33*	This study	2E, S1C
X8743-13A	*MATα srs2-ΔPIM rfa1-t33*	This study	2E, S1C
X8198-15A	*srs2-SIM^{MUT} rfa1-zm2*	This study	2D
X8637-6B	*MATa srs2-7AV::HIS3 rfa1-zm2*	This study	2D
X8137-10B	*MATa srs2-Δ875-902::HPH rfa1-zm2*	This study	2D
X8660-4B	*MATα srs2-2SA rfa1-zm2*	This study	2D
T1358-2	*MATa 8His-SMT3::TRP1*	Lab Collection	5A-B, 5E
X8898-19D	*MATa srs2-Δ::HIS3 8His-SMT3::TRP1*	This study	S2A
X8808-2D	*MATa srs2-ΔPIM 8His-SMT3::TRP1*	This study	5A
X8795-9D	*MATa srs2-3KR::NAT 8His-SMT3::TRP1*	This study	5A
X8807-6A	*MATa sml1Δ::URA3 8His-SMT3::TRP1*	This study	5E
X8746-4D	*MATa sml1Δ::URA3 mec1Δ::TRP1 8His-SMT3::TRP1*	This study	5E
X8807-7A	*MATa sml1Δ::URA3 rad53Δ::HIS3 8His-SMT3::TRP1*	This study	5E
X9055-1D	*MATa DDC2-Myc18::HIS3*	This study	6A, S2B
X9190-8A	*MATa DDC2-Myc18::HIS3 mec1-S1964A*	This study	S2B
X9225-3A	*MATa mec1-S1964A*	This study	6B
X9225-3C	*MATa mec1-S1964A rfa1-zm2*	This study	6B
X9088-38C	*MATa mec1-S1964A srs2-ΔPIM*	This study	6B
X9225-1B	*MATα mec1-S1964A srs2-ΔPIM rfa1-zm2*	This study	6B
X8495-5D	*MATa rfa1-S178D*	This study	6C
X8495-2D	*MATa srs2Δ::HIS3 rfa1-S178D*	This study	6C
X8494-3B	*MATa rfa1-S178A*	This study	6C
X8494-3A	*MATa srs2Δ::HIS3 rfa1-S178A*	This study	6C

X8658-14-22D	*MATa rfa2-3SA*	This study	6D
X8658-14-13C	*MATa srs2Δ::HIS3 rfa2-3SA*	This study	6D
X8779-13D	*MATa rfa2-3SD*	This study	6D
X8779-13B	*MATa srs2Δ rfa2-3SD*	This study	6D
X9265-4D	*MATa SLX4-TAP::HIS3*	(Wan *et al.*, 2019)	4A-C
X9265-4A	*MATa srs2-ΔPIM SLX4-TAP::HIS3*	This study	4A-C
X8956-7C	*MATa slx4^{RIM}-TAP::HIS3*	(Wan *et al.*, 2019)	4A-C
X8956-5D	*MATa srs2-ΔPIM slx4^{RIM}-TAP::HIS3*	This study	4A-C
X9228-2D	*MATa mec1-S1964A srs2-3KR::NAT*	This study	S3A
X9228-5A	*MATα mec1-S1964A srs2-3KR::NAT rfa1-zm2*	This study	S3A
X9090-9C	*MATa mec1-S1964E*	This study	S3B
X9091-14A	*MATa mec1-S1964E rfa1-zm2*	This study	S3B
X9090-19A	*MATa mec1-S1964E srs2-ΔPIM*	This study	S3B
X9132-15B	*MATa mec1-S1964E srs2-ΔPIM rfa1-zm2*	This study	S3B
X9091-13A	*MATa mec1-S1964E srs2-3KR::NAT*	This study	S3B
X9132-10B	*MATα mec1-S1964E srs2-3KR::NAT rfa1-zm2*	This study	S3B
X9137-3B	*MATa mec1-S1964A 8His-SMT3::TRP1*	This study	S3C
X9136-2B	*MATa mec1-S1964E 8His-SMT3::TRP1*	This study	S3C
X9486-5B	*MATa his3::pRS303-p500-SRS2::HIS3 srs2Δ::KanMX*	This study	S4
X9485-8D	*MATa his3::pRS303-p500::HIS3 srs2Δ::KanMX*	This study	S4
X9485-8B	*MATa rfa1-zm2 his3::pRS303-p500::HIS3 srs2Δ::KanMX*	This study	S4
X9486-1D	*MATa rfa1-zm2 his3::pRS303-p500-SRS2::HIS3 srs2Δ::KanMX*	This study	S4
X9484-9C	*MATa rfa1-zm2 his3::pRS303-p500-Srs2-Y775A::HIS3 srs2Δ::KanMX*	This study	S4
X9484-18D	*MATa his3::pRS303-p500-Srs2-Y775A::HIS3 srs2Δ::KanMX*	This study	S4